Experimental Investigation of Flow Boiling Instability

in a Single Vertical Microtube:

Effects of Hydraulic Diameter and Flow Orientation

Qian You

A Thesis

in

The Department

of

Mechanical and Industrial Engineering

Presented in Partial Fulfillment of the Requirements

For the Degree of Master of Applied Science (Mechanical Engineering) at

Concordia University

Montréal, Québec, Canada

December 2014

CONCORDIA UNIVERSITY
School of Graduate Studies

This is to certify that the thesis prepared

By: Qian You

Entitled: Experimental Investigation of Flow Instability in a Single Vertical Microtube: Effects of Hydraulic Diameter and Flow Orientation

and submitted in partial fulfillment of the requirements for the degree of

Master of Applied Science (Mechanical Engineering)

complies with the regulations of the University and meets the accepted standards with respect to originality and quality.

Signed by the final examining committee:

Dr. Robin Drew Chair

Dr. Hoi Dick Ng Examiner

Dr. Nizar Bouguila Examiner

Dr. Ibrahim Hassan and Dr. Lyes Kadem Supervisor

Approved by _____

Chair of Department or Graduate Program Director

_____

Dean of Faculty

Date December 19, 2014

Abstract

Experimental Investigation of Flow Boiling Instability in a Single Vertical Microtube:

Effects of Hydraulic Diameter and Flow Orientation

Qian You

Concordia University 2014

Flow boiling in a microchannel heat sink is considered as a suitable and an efficient method to dissipate high heat flux from a small surface. Especially, this technique can achieve uniform axial temperature distribution and low noise with a little coolant and low pumping power consumption. However, the main drawback of this attractive technique is flow instability which is induced by the flow phase change. Flow instability can constrain the advantages of flow boiling heat transfer, or even damages systems.

In this thesis, the fundamental investigations on the flow instability in a single vertical microtube are conducted. The objectives are to understand the flow oscillations types and features in vertical flow directions, the effects of geometric factors (hydraulic diameter of microtube and flow orientation) and operating conditions (mass flux and heat flux) on flow instability behaviors, and to investigate the inlet orifice for controlling flow instability in vertical flow directions. Three different sizes of stainless steel microtubes with 0.305, 0.533 and 0.889 mm hydraulic diameters are tested. The working fluid FC-72 maintains around 24 °C at the inlet of microtube. The mass flux varies from 700 to 1600 kg/m^2·s, and the heat flux is applied on the tube surface uniformly up to 9.6 W/cm^2. For the flow instability controlling study, two sizes of inlet orifices (50% and 20% area ratio)

are investigated, respectively. The experimental results show that in a large hydraulic diameter, the onset of flow instability with obvious and sustained oscillation features is usually observed, and it can be delayed by large mass fluxes. In a small hydraulic diameter, the transient point is most detected and occurs earlier than in large size microtubes at a given mass flux, and the mass flux effect on its occurrence can be ignored. The buoyancy force impacts the flow instability appearance and characteristics. The irreversible flow blockage is observed in the smallest tube in downward flow direction and not sensitive to the mass flux. With more heat flux applied on the largest tube, the flow oscillations change to intensive in upward flow direction, but tend to be re-stabilized in downward flow direction. The 50% inlet orifice shows better performance at large mass fluxes or in upward flow direction. The 20% inlet orifice has a good ability to eliminate flow instability in the current investigation, but it induces higher pressure drop than 50% inlet orifice.

Acknowledgements

I would like to give my special thanks to my supervisor Professor Ibrahim Hassan and co-supervisor Professor Lyes Kadem for their expert knowledge and advice, encouragement throughout this study, and extraordinary supports in this thesis.

I also would like to thank my friend, former team member, Dr. Yanfeng Fan for helping in the lab and precious comments in this thesis. Thanks to my colleagues Amen, Ming and Yingjie to contribute their valuable suggestions and time. Thanks to my dear friends Jing Chen, Jian Liu and Sui Jiang (Shawn) Si Tu for their friendships in my life and my study.

Last, I would like to thank to my parents for everything. No matter what happened, you are always there to fully support me and raise me up.

Table of Contents

List of Figures

List of Tables

Nomenclature

A_h microtube inner area (mm^2)

A_o inlet orifice inner area (mm^2)

C_p thermal capacity (J/kg·°C)

D_h microtube hydraulic diameter (mm)

D_o inlet orifice hydraulic diameter (mm)

f   frequency (Hz)

G   mass flux (kg/m^2·s)

g   gravitational acceleration

I   current (A)

L   microtube length (mm)

L_h microtube heated length (mm)

L_o inlet orifice length (mm)

N   number of samples

P   pressure (kPa)

q"   heat flux (W/cm^2)

Q_{loss} heat loss (W)

T   Temperature (°C)

V   voltage (V)

x_i samples

Abbreviation

AMP   amplitude (kPa)

AR   area ratio

DWO   density wave oscillation

L   microtube with large hydraulic diameter 0.889 mm

M   microtube with medium hydraulic diameter 0.533 mm

MAG   magnitude (kPa)

OFI   onset of flow instability

PDO   pressure drop oscillation

S   microtube with small hydraulic diameter 0.305 mm

VD   vertical downward flow direction/configuration

VU   vertical upward flow direction/configuration

Subscript

exp   experimental

i   location of sample point

in   inlet

out   outlet

sat   saturated

tran   transient

w   wall

w/o   without

Chapter 1

1 Introduction

Nowadays, as technology develops rapidly, microelectromechanical systems (MEMS) have attracted more attentions due to their tiny size, powerful abilities and low cost. Many applications have already served commercial and industrial areas. A lab-on-a-chip (LOC) is an exciting example in bio/chemical analysis, which is available for medical diagnosis, environmental pollution monitoring and so on. This technology is still novel and developing. MEMS sensors and actuators in space industry are another essential application to reduce the weight and space of the system, plus save energy and cost. MEMS are also widely used in robotic, automobile and communication industries. However, in the meantime, the heat generated in a unit area (the heat flux) in electronic parts is significantly increased. It may cause system damage and/or control failure. For example, an extremely high flux of 10^4 W/cm^2 in the fusion reactor blanket was reported (Mudawar, 2011). The traditional forced air, heat pipe or submerged cooling methods are not suitable to cool down these devices anymore due to low heat rejection ability, large size, a lot of noise and a large amount of coolant consumption. Therefore, forced convection in a microchannel heat sink is a reliable and suitable solution because it can achieve a high heat transfer coefficient, which is inversely proportional to the channel

1

hydraulic diameter, by using a small amount of coolant to satisfy large heat dissipation from a limited area.

The working fluid in a microchannel heat sink can be either single-phase or two-phase. The single-phase flow forced convection has been investigated extensively in the last decades. Although it can increase heat dissipation in a small area, it requires large pumping power or small channel size since single-phase utilizes sensible heat transfer for cooling. It also brings uneven surface temperature distribution along the working fluid path so that the system performance and the life time are restricted. By comparison, two-phase fluid forced convection has more advantages: (1) significantly higher heat transfer coefficient which can be obtained due to latent heat transfer; (2) reduced pressure drop and amount of coolant; and (3) uniform axial temperature distribution. Hence, flow boiling in microchannels is believed to be an ideal solution for cooling compact size electronic devices with high heat flux generation. However, nothing is perfect; flow instability, the major shortcoming of flow boiling techniques, always exists.

Flow boiling instability in conventional size channels has been widely studied experimentally and numerically. The research results show that it may physically induce mechanical vibration of components or the system control failure, and it also affects the local heat transfer coefficient and may cause local dryout.

In micro scale studies, the flow boiling heat transfer mechanisms are proved different from the conventional size since the surface tension is dominant. In the same way, the flow instability is required numerous investigations to understand its characteristics to affect the system performance, and then to be controlled and/or eliminated. Among these investigations, the fundamental ones in a single microchannel are very important. Since

removing the physical phenomena induced by disturbances between multiple channels, the nature of flow instability can be better observed. Most researches have been previously investigated in horizontal configurations. The flow instability in different hydraulic diameters is short of experimental results which are important for optimizing microchannel heat sink design. Besides, the flow orientation effect on flow instability is rarely discussed but it is essential for future practical application design.

The present study aims to fundamentally investigate the flow instability in a single microtube regarding the effects of the hydraulic diameter and the flow orientation. Chapter 2 summarizes recent researches related to flow boiling instability in mini/microchannels, especially, forcing on researching points of this project. Chapter 3 introduces the experimental setup, the measurement methodology and the uncertainties. Chapter 4 discusses the experimental results of the flow oscillation types and characteristics in different hydraulic diameters, and the studies of operating condition effects are included. Chapter 5 compares the flow instability in vertical upward and downward flow orientations, and investigates the inlet orifice on flow instability control in vertical flow directions. Chapter 6 concludes the current work and the prospects of the future researches.

Chapter 2

2 Literature Review

This chapter reviews recent literatures and publications on the flow boiling in microchannels. The investigations on the bubble dynamics and flow patterns which are considered as the main sources of flow boiling instability are discussed. Furthermore, the parameters expected to affect the flow boiling instability, including flow orientation, hydraulic diameter are highlighted. The flow instability stabilization researches are summarized as well.

2.1 Bubble Dynamics

In modern studies on flow boiling in microchannel(s), there are two methods to achieve flow boiling: two-phase entry and subcooled liquid entry. In reality, two-phase flow is hard to be controlled and stabilized before entering micrcochannels since the vapor blockage leading to uneven flow distribution may be induced. Single-phase liquid, by contrast, is easy to be operated and controlled before entering microchannels; therefore, this method is more attractive and the most widely investigated. Since the phase changing occurs inside of microchannels, the bubble dynamics, including bubble nucleation,

growth and departure, is important. This leads to flow pattern formation which not only enhances the heat transfer coefficient but also induces flow oscillations. Hence, many researchers investigated the origin of flow boiling, heat transfer mechanism and two-phase pressure drop in microchannels.

Kandlikar (2014) performed studies of bubble nucleation in mini/microchannels. As shown in Figure 2.1, the wall temperature T_w, resulting from the application of a heat flux on the tube surface, is larger than the saturated temperature of the working liquid $T_{L,sat}$; small cavities may act as nucleation sites which can trap vapor or gases, and the trapped vapor or gases starts to growth. The pressure of the vapor p_v and the pressure of the liquid p_L are balanced by the surface tension force σ,

$$p_v - p_L = \frac{2\sigma}{r_b} \tag{2.1}$$

where r_b is the bubble radius. The liquid temperature at $y = y_b$, has to be larger than the saturated temperature of liquid corresponding to the pressure p_v to maintain the bubble, which is also a condition for nucleation,

$$T_{L,y_b} \geq T_{L,sat(p_v)} \tag{2.2}$$

In conventional channels with boiling flow, various forces have been considered acting on bubbles to control their growth and departure, including the inertial force, the surface tension, the buoyancy force and the drag force (Levy, 1967). In microchannels, the surface tension becomes dominant. The surface tension force tends to maintain bubbles on the channel surface, while the drag force impels bubbles to depart from nucleation sites. The buoyancy force is usually negligible (Kandlikar, 2014).

Bogojevic et al. (2013) conducted experiments to investigate the bubble dynamics in water flow boiling in a horizontal rectangular microchannel heat sink with 0.194 mm hydraulic diameter. They observed three stages for bubble growth: a rapid growth initial stage controlled by inertia forces, a slow growth second stage controlled by thermal diffusion, and a rapid growth last stage caused by the bubble confinement led to enhanced evaporation. They also concluded that the bubble departure size decreased with surface tension induced by high heat flux, and as the drag force increased caused by high mass flux. In a flow visualization experiment, they observed that flow instabilities were mainly due to the existence of revered flow induced by rapid growth of a confined bubble.

Yin et al. (2014) carried out experiments to investigate bubble confinement and elongation in a single rectangular microchannel with 0.667 mm hydraulic diameter and 100 mm heated length. The authors studied the effect of mass flux, heat flux and subcooled inlet temperature in water flow. Based on the experiment data and flow visualization results, they concluded that bubble growth rate during free growth period was smaller than during confined growth period. Moreover, before bubble confinement,
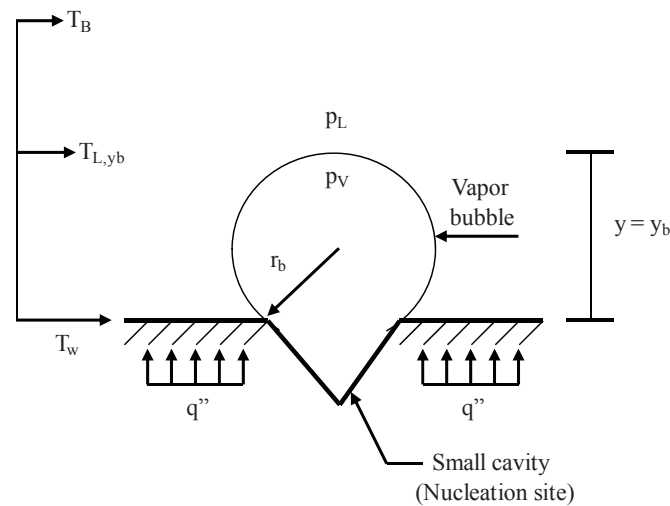
Figure 2.1: The schematic of bubble nucleation site

bubble growth rate decreased with the increase in bubble size; after bubble confinement, the elongation rate increased with the increase in confined bubble size.

Edel and Mukherjee (2011) carried out experiments to visually investigate bubble growth in flow boiling in a single horizontal microchannel (hydraulic diameter D_h = 0.229 mm) at low mass fluxes. They observed that when the drag force was enough to overcome the surface tension, the bubbles would start to detach from the wall or slide along the wall surface before confined by the channel. In contrary, when the surface tension was dominant and the growing bubble reached the channel size before moving, it tended to expand in one or two direction(s) according to the mass flux. The authors also recorded the real time surface temperature oscillations with large amplitudes and low dominant frequency during unstable flow boiling.

Two research teams Barber et al. (2010) and Wang et al. (2011a) from the same group investigated bubble confinement in an identical single microchannel with a high aspect ratio (D_h = 0.727 mm). FC-72 was selected as the working fluid. The former detected that the confined bubbles blocked the channel and caused sharp pressure fluctuations at both ends of the microchannel. The latter found that the increased heat flux or the decreased mass flux led to a decreasing pressure drop fluctuation dominant frequency.

Kadam et al. (2014) simplified the numerical model to predict bubble growth at nucleation site in microchannels. The authors derived an energy balance equation for the vapor phase. They assumed that the heat consumed in vapor phase was from bubble growth and was used for overcoming resistive forces, such as surface tension, inertia, shear, gravity and changing in momentum due to evaporation. The authors noted that the

bubble growth was dependent on operating conditions (the mass flux and the heat flux), the coolant properties and the channel geometry.
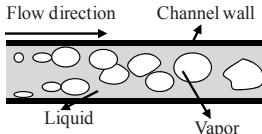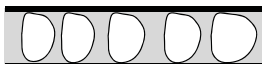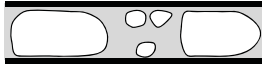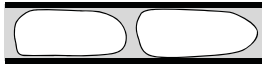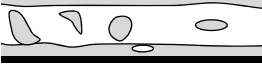
2.2 Flow Patterns

In small hydraulic diameter channels, the surface tension becomes more dominant. Once the bubble nucleation starts, bubble growth and/or confinement induce(s) different flow patterns formed according to the flow conditions. With the rapid development in visualization techniques, many studies investigated flow pattern regime mappings under different operating conditions. This is essential for predicting heat transfer rate and working limitations. Table 2.1 lists common flow patterns in micro scale channels from several previous research groups.

In early flow visualization studies in small channels, Shuai et al. (2002) conducted experiments to study pressure drop and heat transfer of flow boiling in two single rectangular channels (D_h = 0.800 and 2.67 mm) with subcooled water in vertical upward flow direction. Different operating conditions were applied: a heat flux varying from 1.8 to 10.0 W/cm^2 and a mass flux varying from 200 to 700 $kg/m^2 \cdot s$. Three basic flow patterns in both channels were observed: bubbly flow, slug flow and annular flow under different operating conditions, and these flow patterns were found to co-exist along the channel. The authors reported the pressure drop fluctuations they observed, and assumed that these fluctuations could be related to the flow patterns.

Sobierska et al. (2006 and 2007) from the same research group investigated and discussed the flow and the heat transfer characteristics in single vertical rectangular mini/microchannels with the upward water flow direction. The former team performed

Table 2.1: Typical flow patterns in mini/microchannel(s)

Typical Flow Patterns	Description
Flow direction Channel wall Liquid Vapor	**Isolated Bubbly Flow** Distinct and essentially spherical bubbles and, usually have smaller diameters than the channel.(Martin-Callizo et al., 2010)
	Confined Bubbly (Elongated Bubble) Flow Distinct but distorted (non-spherical) bubbles which were restricted by the channel walls. The bubbles started growing in the axial direction. (Martin-Callizo et al., 2010; Ali et al., 2013)
	Bubbly/Slug Flow Bubbles grew to the channel width, moved downstream while growing in the flow direction, and finally formed slug and elongated bubbles within a few milliseconds. (Huh et al., 2007)
	Slug Flow Elongated, bullet-shaped bubbles with spherical cap and flat tail (slugs) that occupy most of the cross section. In this regime, the liquid flow is mainly contained in liquid plugs, which separate successive vapor slugs. The liquid plugs may or may not contain smaller bubbles. (Martin-Callizo et al., 2010)
	Churn Flow Churn flow is formed when the vapor slugs become unstable and disrupted. The vapor flows in a more or less chaotic manner through the liquid, which is mainly displaced to the channel wall. (Martin-Callizo et al., 2010)
	Wispy-annular Flow A vapor core which contains large, irregular-shaped liquid droplets inside is separated from the channel wall with a relatively thick and unstable liquid film. (Harirchian and Garimella, 2009)
	Slug-annular Flow The collision of neighboring slugs leading to a wavy-annular flow pattern with deep waves that interrupt the annular flow. (Martin-Callizo et al., 2010)
	Annular Flow The gas flows continuously in the tube center while the liquid flows in a film along the channel wall. (Martin-Callizo et al., 2010)
	Mist Flow Mist flow is with the majority of the flow entrained in the gas core and sipersed as liquid droplets. (Martin-Callizo et al., 2010)

experiments in a channel with 1.20 mm hydraulic diameter and 300 mm heated length. The tested mass fluxes ranged between 50 and 1000 $kg/m^2 \cdot s$, and the maximum heat flux applied was 10 W/cm^2. With the help of flow visualization, they observed bubbly, slug and annular flows, and that the transition flows co-existed in the channel. The authors calculated the mass flux versus the vapor quality regarding flow patterns and concluded that bubbly flow mainly occurred at subcooled condition. The vapor quality was found to increase as the mass flux decreased. Then, the later team carried out experiments in a smaller channel with 0.480 mm hydraulic diameter at a mass flux varying from 200 to 1500 $kg/m^2 \cdot s$. The heat fluxes were applied in the range of 3 to 20 W/cm^2. Flow patterns observed were consistent with the group previous work; moreover, the authors observed that the annular flow occurred at a low vapor quality and the bubbly/slug transition was at subcooled condition. Furthermore, the authors concluded that bubble nucleation was postponed by increasing mass flux.

Harirchain and Garimella (2009) investigated the effect of channels size on flow patterns in rectangular microchannel heat sinks. They designed seven test sections which contained 0.400 mm depth multiple channels but with different widths to form a series of hydraulic diameter from 0.160 to 0.749 mm. Then, the authors built up a flow pattern map based on their observations, including bubbly, slug, churn, wispy-annular, annular and inverted annular flow (post-dry-out). Additionally, they found that the channel width affected the dominant flow patterns. In small channels (D_h = 0.160 and 0.400 mm), slug and intermittent churn/annular flows were more often observed; however, in large channels, bubbly and intermittent churn/wispy-annular flows were dominant. Nevertheless, the authors noticed that the onset of bubble nucleation occurred at a higher

10

heat flux as the mass flux increased.

Kandlikar (2010) gave a fundamental review on scaling studies on flow boiling heat transfer in microchannels. He indicated that the flow patterns were influenced by various kinds of forces, including surface tension, inertia, shear, gravity, bubble nucleation and evaporation. Also, he concluded that elongated bubble/slug flow pattern was dominant in microchannels.

Recently, Ali et al. (2013) visually investigated the flow patterns and the bubble dynamics in a single horizontal microchannel with 0.781 mm hydraulic diameter and 191 mm heated length at low mass fluxes (from 100 to 400 kg/m^2·s). R134a was selected as the working fluid, and the applied heat flux was up to 4.5 W/cm^2. The authors described seven distinct flow patterns based on their observations during experiments. Isolated bubble flow, confined bubble flow, elongated bubble flow, slug flow, wavy annular/semi annular flow, annular flow, annular mist flow and mist flow were on the list. They found that the early transition from the bubbly flow to the elongated bubble/slug pattern in small channels is due to early bubble confinement. The authors compared their work with a previous study of Martin-Callizo et al. (2010) using the same experiment facility but in a vertical channel with a hydraulic diameter of 1.33 mm. They concluded that in small channel dimensions, the flow orientation might has negligible effect on the flow patterns evolution, but they suggested that future works are required to confirm this conclusion.

Simultaneously, some researchers were interested in the flow pattern transitions which might induce flow boiling instability in microchannels. Wang et al. (2007) designed experiments to study the flow stable regimes in both single and multiple trapezoidal microchannel(s) with a hydraulic diameter 0.186 mm and subcooled water

11

inlet. In a study on multiple microchannels, the heat fluxes applied were up to 49.78 W/cm^2. The authors detected a stable flow boiling regime when the heat and mass flux ratio was low (q"/G < 0.96 kJ/kg). At a given heat flux, isolated bubbles, elongated bubbles, bubble coalescence, and bubble expansion in both upstream and downstream directions were respectively observed as the mass flux decreased. At the meantime, subcooled outlet temperature was recorded during this stable regime. There were two unstable flow boiling regimes, one with long-period oscillations (0.96 kJ/kg < q"/G < 2.14 kJ/kg) and the other with short-period oscillations (q"/G > 2.14 kJ/kg). Via flow visualization, the authors noticed that bubble expansion inducing flow pattern transitions from bubbly flow to annular/mist flow was the main reason causing long-period oscillations. The mist flow transition to annular flow was observed in short-period oscillations. In a study on a single microchannel, the applied heat flux was up to 29.78 W/cm^2. The stable flow boiling regime was found similar to multiple-channel case; however, long-period oscillations were milder than in multiple channels; the authors explained that this was due to flow interaction from neighboring channels leading to extra oscillations in multiple-channel case. In addition, they concluded in both single and multiple microchannel(s), that the amplitude and the frequency of inlet pressure oscillations were increased with increased heat flux; however, mass flux had no impact on the frequency.

Steinke and Kandlikar (2004) performed flow visualization to study flow boiling characteristics in a horizontal microchannel heat sink with 0.207 mm hydraulic diameter. The subcooled water entry was tested. Various flow patterns were observed. The authors reported that the bubbly flow was very intermittent. The annular-slug and the slug flow

were the most common observed flow patterns. They also found that the bubble expanded

against the flow direction when the annular-slug flow was formed.

Chen et al. (2006) presented the flow pattern images in four tubes with different sizes

in vertical upward flow direction. In the smallest one (D_h = 1.10mm), the dispersed

bubble, the bubbly, the confined bubble, the slug, the churn and the annular flow patterns

were observed. The confined bubble flow was reported only occurring in small tubes.

The authors noted the surface tension force became dominant in small tubes at low mass

fluxes.

Huh et al. (2007) also conducted flow pattern transition instability experiments in a

single rectangular horizontal microchannel. The channel hydraulic diameter was 0.104

mm and the heated length was 40 mm. Within the test ranges of mass fluxes (170 and 350

$kg/m^2 \cdot s$) and heat fluxes (20 to 53 W/cm^2), the authors recorded periodic flow pattern

transitions: alternation of bubbly/slug flow and alternation of elongated slug/semi-annular

flow. Then, the flow pattern transition instability was considered as the major source

causing periodic small frequency and large amplitude oscillations of wall temperature,

pressure drop, and mass flux.

Celata et al. (2010) plotted the flow stable regime within the test matrices (mass flux

up to 3500 $kg/m^2 \cdot s$ and heat flux up to 20 W/cm^2) in a single horizontal microtube (D_h =

0.480 mm) with subcooled FC-72 liquid inlet. Bubbly, bubbly/slug, slug, slug/annular,

and annular/mist flow were observed. Nevertheless, the authors recorded the stable and

unstable flow regimes during flow boiling according to different operating conditions.

There were two stable flow zones: alternating bubbly/slug flow in the case of high mass

flux and low heat flux; alternating annular/slug flow and alternating annular/mist flow in

the case of low mass flux and high heat flux. In the unstable flow zone, alternating annular/slug flow were observed at low heat flux and alternating bubbly/slug flow at high heat flux. Furthermore, a kind of back and forth oscillations was noted at low mass and heat fluxes but no reversed flow occurred.

2.3   Flow Instability

Flow boiling in mini/microchannels is a two-edge sword. On one hand, it enhances the heat transfer coefficient. On the other hand, flow boiling instability impacts flow characteristics and heat transfer negatively. Comprehensive studies on flow instability in conventional channels have already been performed since decades in conventional channels (macro-scale). Several research teams have shown; however, that the results obtained for convenctional channels cannot be applied to mini/micro-scale cases. Therefore, some researchers built up maps of flow stability regimes based on their experimental results to exhibit stable and unstable flow regimes in mini/micro-scales (Brutin et al., 2003; Wang and Cheng, 2008). Some of them recorded the real-time pressure and temperature fluctuations to analyze the flow oscillation types (Xu et al., 2005; Fan and Hassan, 2012). These research topics have also been extended to the effects of operating conditions and other parameters (channel geometry, coolant type and so on). Moreover, the flow instability control/elimination is another important objective.

2.3.1   Onset of Flow Instability Investigations

The onset of flow instability (OFI) has been previously studied in conventional channel

sizes (Whittle and Forgan, 1967; Lee and Bankoff, 1993). Whittle and Forgan (1967) defined the occurrence of Ledinegg instability based on the characteristics of the pump supply - the system demand curve; that is, if the pump operating condition could not fulfill the power required in the system, the Ledinegg instability was triggered, as shown in Figure 2.2. For example, at a given heat flux q"$_2$, the flow was stable under the operating condition on the right side of OFI. After reducing the mass flux, the flow became unstable. Boure et al. (1973) summarized the Ledinegg instability leading to a sudden flow rate drop could occur if the condition of Eq. (2.3) was satisfied. They also mentioned that Ledinegg instability could trigger another steady-state condition or a periodic behavior (such as dynamic instabilities). Therefore, the occurrence of Ledinegg instability can be considered as the OFI.

$$\left.\frac{\partial P}{\partial G}\right|_{demand} \leq \left.\frac{\partial P}{\partial G}\right|_{supply} \tag{2.3}$$

Kennedy et al. (2000) collected 70 experiments data in two sizes of horizontal microchannels (D_h = 1.17 and 1.45 mm) with 160 mm heated length. Then, they generated a simple empirical correlation (Eq. (2.4)) to predict heat fluxes at OFIs within a wide mass flux range (from 800 to 4500 kg/m^2·s),

$$q"_{OFI} = 0.9 q"_{sat} \tag{2.4}$$

In this correlation, the predicted heat flux at OFI is 90% of its saturated value at the exit of that channel under identical operating conditions.

Roach et al. (1999) conducted experiments by using the same facility and test sections as the investigation of Kennedy et al. (2000), but at lower mass fluxes (from 220 to 790

kg/m^2·s). The authors also proposed a similar correlation based on 95 sampling data to predict heat fluxes at OFIs but with a constant of 1.1 (Eq. (2.5)),

$$q''_{OFI} = 1.1 q''_{sat} \tag{2.5}$$

The saturated value in both correlations (Eq. (2.4) and (2.5)) can be obtained by Eq. (2.6),

$$q''_{sat} = \frac{D_h}{4L_h} G \cdot C_p \left(T_{sat} - T_{in} \right) \tag{2.6}$$

where D_h is the channel hydraulic diameter, L_h is the channel heated length, G is the mass flux, C_p is the thermal capacity of the coolant, T_{sat} is the saturated liquid temperature, and T_{in} is the inlet temperature.

Wang et al. (2011b) studied some specific points including OFI on demand characteristic curves in a narrow rectangular channel in vertical upward flow direction. The channel with 5.58 mm hydraulic diameter was single-side heated with 470 mm heated length. The mass flux was in the range between 150 and 600 kg/m^2·s. They
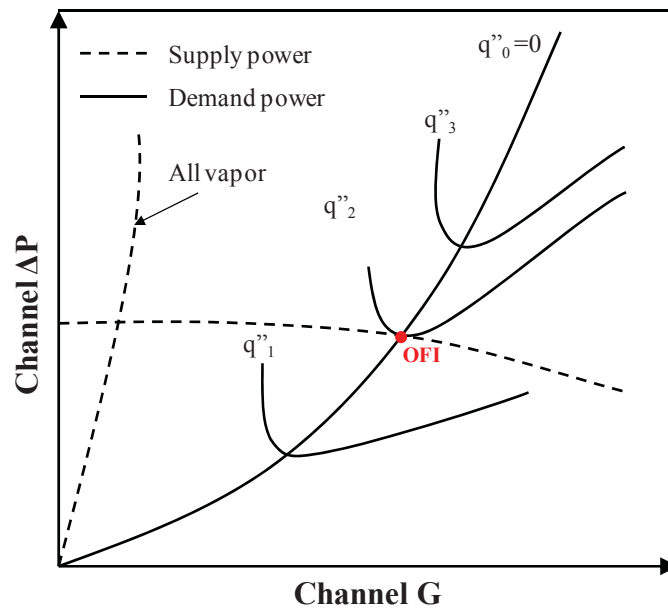
Figure 2.2: The typical pressure drop – flow rate characteristics curve

used the correlation proposed by Kennedy et al. (2000) for OFI prediction to verify their experimental results, and it showed a good agreement. Via flow visualization, the bubbly, the churn and the annular flow were observed, but excluded the slug flow. The authors noticed that the OFI always appeared when the bubble started coalescing at the channel outlet. They also mentioned that the OFI might be relevant to the beginning of the bubbly/churn flow pattern transition.

2.3.2 Effect of the Channel Size

In mini/microchannels, only few researches regarding the channel size or aspect ratio effect on flow boiling instabilities have been conducted.

Wu and Cheng (2003) visually investigated the flow boiling instability in two sizes of microchannel heat sinks. Both test sections contained parallel trapezoidal microchannels but with different hydraulic diameters, 0.083 and 0.159 mm, respectively. In the larger microchannel heat sink, the authors recorded periodic oscillations at the mass flux of 144 kg/m^2·s, and the heat flux was 13.0 W/cm^2. The single-phase liquid and the two-phase flows were observed alternatively in microchannels once boiling occurred. Meantime, the channel wall temperature experienced low frequency and large amplitude oscillations. In the small microchannel heat sink, the authors recorded that flow boiling instability occurred for a mass flux of 168 kg/m^2·s, and a heat flux was 7.83 W/cm^2. They noticed that in small channels, the slug and the churn flows occurred more easily. After comparing flow oscillation characteristics in both microchannel heat sinks, they concluded that the oscillation frequency was dependent on channel size and operating conditions.

Qi et al. (2007) conducted experiments to investigate flow boiling instabilities in different sizes of single microtubes. Those microtubes had 0.531, 0.834, 1.042 and 1.931 mm hydraulic diameters, respectively, and identical heated length of 191 mm. Liquid nitrogen was selected as the working fluid. A wide range of mass fluxes from 440 to 3000 kg/m^2·s were tested. The heat flux was applied up to 21.4 W/cm^2. The authors described the onset of nucleate boiling (ONB) as the phenomena responsible for the sudden drop in mass flux, and in the increase in pressed drop. They observed that ONB first occurred at the channel outlet, and gradually moved to the channel inlet as the heat flux increased, and so did the wall temperature at ONB. The flow blockage at ONB was observed as well. The authors explained that it might be due to the slower bubble discharging rate than the bulk fluid rate, and local dryout might be induced. In the 1.042 and 1.931 mm hydraulic diameter tubes, the stable and unstable regimes were detected. In the smaller one (D_h = 1.042 mm), the critical mass flux to distinguish flow stable regimes was smaller than that in the larger one (D_h = 1.931 mm). For other two smaller sizes of microtubes, no unstable regimes were detected since the applied mass fluxes were lower than the critical values.

Hetsroni et al. (2006) carried out experiments in microchannel heat sinks with different hydraulic diameters (D_h = 0.100, 0.130 and 0.220 mm) to study the flow boiling instability at low mass fluxes. The mass flux and the channel hydraulic diameter affecting on the ONB location were reported. At a given mass flux, the ONB location was closer to the channel inlet as the heat flux increased. At a given heat flux and inlet temperature, the ONB moved further from the channel inlet as the hydraulic diameter increased. The authors observed periodic oscillations of pressure drop and fluid temperature when the

minimum film thickness at CHF regime occurred.

2.3.3 Effect of the Flow Orientation

Kandlikar and Balasubramanian (2005) studied the effect of flow orientation on the flow boiling instability of water in a rectangular minichannel heat sink (D_h = 0.333 mm). The flow visualization in horizontal, vertical upward and vertical downward flow directions was performed under one operating condition (G = 120 kg/m^2·s and q" = 31.7 W/cm^2). The authors observed different flow patterns, such as bubbly, plug and annular flows, in all three flow directions, and reported the churn flow which was not widely, previously observed in the literature. They noticed that the flow patterns were time dependent. In the horizontal flow direction, an individual bubble growing to a vapor slug was observed. However, in the vertical flow orientations, bubble merged and then formed a vapor slug. A revered flow was recorded in all flow directions, but it was more distinct in the vertical downward flow. The pressure drop oscillations in the vertical upward flow were the smallest; therefore, the flow was considered less chaotic in that configuration. Compared the local heat transfer coefficients in all flow orientations, the authors concluded that the cases in vertical upward and horizontal flow directions were similar, but in the vertical downward flow, the local heat transfer coefficient was 30% to 40% lower.

Zhang et al. (2005) reviewed previous works and concluded the flow instabilities and flow orientations might affect heat transfer in microchannels. Therefore, they conducted experiments to visually and quantitatively study the flow boiling in a microchannel heat sink with three flow orientations (horizontal, vertical up and down). The test section contained 21 rectangular microchannels which had 0.360 mm hydraulic diameter and 15

19

mm heated length. The dielectric coolant FC-72 was tested with subcooled inlet entry. In the vertical downward flow direction, the authors observed three sizes of bubbles. Tiny ones located close to channel inlet. They were usually attached to the channel wall and moved at very slow speed. The largest bubbles were found a few millimeters from the inlet which were formed by tiny bubbles coalescing and moved with a higher speed but still lower than the bulk fluid because of the buoyancy force effect. The moderate bubbles were formed by growing bubbles and had the fastest speed. According to their observations and the investigations from previous studies, the authors predicted single-phase liquid might suddenly turn to annular flow without transitional regimes in small channel (D_h < 0.100 mm). Additionally, the transient thermal resistance and pressure drops in three flow orientations were compared. The vertical upward configuration performed the best due to buoyancy force assisting bubble movement. In contrary, the vertical downward configuration induced the highest pressure drop.

Miyata et al. (2008) performed flow boiling studies in a single small cooper tube (D_h = 1.00 mm) using R410A refrigerant. The tube was tested vertically in both upward and downward flow directions with 320 mm heated length. The mass flux varied from 30 to 200 kg/m^2·s, and the heat flux was applied up to 1.6 W/cm^2. Three flow patterns were observed in both flow directions: the slug, the slug/annular and the annular flows. They noted an early transition from the slug flow to the annular flow at low mass flux condition in the vertical downward flow direction. The authors reported that the pressure drops in the downward flow direction was significantly larger than in the opposite direction, and they explained that the vapor plug boiling in the liquid flow might be the reason for the increase in pressure drop in downward direction.

Wang et al. (2012) designed an experiment to investigate the effect of flow orientation on flow boiling behaviors in a microchannel heat sink by using HFE-7100 coolant. The heat sink had multiple parallel rectangular microchannels with 0.825 mm hydraulic diameter, and was placed in different orientations from vertical upward to vertical downward. The authors observed that the slug velocity was increased in the upward flow direction due to the buoyancy force effect. They concluded that at low mass fluxes or low vapor quality, the flow orientation had impacts on the flow patterns.

2.3.4   Effect of the Inlet Orifice

Brutin and Tadrist (2004) tested two inlet conditions for flow boiling instability control in a single vertical rectangular minichannel (D_h = 0.889 mm). Confinement case was selected to maintain constant mass flux at the inlet of the test section. Compliance case was pointed to maintain constant mass flux at the outlet of the syringe. This was accomplished by installing a compressible buffer tank between the syringe and the test section. The authors reported that for the same operating conditions, the amplitude of pressure drop oscillations in the compliance case was higher than that in the confinement case.

Kandlikar et al. (2005) introduced a combination of an inlet pressure restrictor (PDE) and artificial nucleation sites to stabilize flow boiling instability. They performed three different stabilization cases to compare the pressure drop oscillations in a heat sink with 0.333 mm hydraulic diameter. In the case of artificial nucleation site only, the flow instability was not controlled. In the case of 51% area PDE with artificial nucleation sites, the flow oscillations were partially controlled. Then, in the case of 4% are PDE with

artificial nucleation sites, the flow instability was totally eliminated; however, the pressure drop was significantly increased.

Wang et al. (2008) carried out experiments to study three flow restriction configurations for flow boiling stabilization for one identical operating condition. The test section was a microchannel heat sink with trapezoidal cross-section shape, and its hydraulic diameter was 0.186 mm. Experimental results showed that in both inlet and outlet flow restrictor case, the amplitudes of temperature and pressure drop were higher than in the no flow restrictor case. However, only with the inlet flow restrictor case, the flow instability could be totally controlled. Moreover, the authors visualized the bubble/annular flow regimes during flow instability in the case without flow restrictors.

Mukherjee and Kandlikar (2009) numerically investigated the effect of the inlet restrictor on flow boiling instability in microchannels. They mentioned that the major source responsible for flow boiling instability in small size channel was the reversed flow due to rapid vapor growth rate to expend in both upstream and downstream directions, and upstream induced high pressure buildup. Therefore, a sufficient flow rate or an inlet restriction was needed for overcoming the reversed flow. The inlet orifice was recommended to increase inlet flow velocity in order to reduce the bubble growth rate. The authors found that 4% area ratio inlet restrictor could eliminate the flow instability; however, this increased the pressure drop at the meantime. Therefore, they proposed stepped and diverging parallel microchannels in order to prevent extra pressure drops.

Park et al. (2009) conducted experiments to visually investigate the flow instability and the inlet orifice effect in a microchannel heat sink. The heat sink contained parallel rectangular microchannels with high aspect ratio (0.467 mm $\times$ 4.052 mm, D_h = 0.837

mm). The authors observed the reversed flow when no inlet orifice was involved. Then, they visualized the inlet orifice could suppress the reversed flow. The flashing effect was also reported in the case of with-inlet-orifice using R134a, which had advantages to reduce the wall-temperature overshoot at the onset of boiling.

Fan and Hassan (2012) performed a fundamental investigation in a single horizontal microtube (D_h = 0.889 mm) with and without inlet orifice. The authors observed four types of flow oscillations when no inlet orifice was present. When added the inlet orifices, by comparing the flow characteristics and the pressure drop, they recommended that a 20% area ratio (inlet orifice cross-section area/microtube cross-section area) could be used at low mass fluxes (< 1000 kg/m^2·s). Later, Fan and Hassan (2014) proposed a methodology to predict the onset of flow instability in a single horizontal microtube based on their previous experimental results in order to select proper inlet orifice sizes. The authors suggested that: at a given mass flux, when the two-phase pressure drop in the microtube with the heat flux applied was higher than the single-phase pressure drop without heat flux applied, the flow instability appeared. As an example: for a microtube with the hydraulic diameter 0.889 mm, 15% area ratio inlet orifice could completely eliminate the flow instability in the mass flux range from 100 to 2000 kg/m^2·s.

2.4 Summary and Objectives

To sum up the previous studies,

- Although many groups investigated the flow stable regimes, the regimes were specific under different geometrical and operating conditions. A universal flow

pattern regime map in terms of dimensionless parameters is absent. This tool can be valuable for microchannel heat sink design and/or optimization.

- Flow instability is a critical limit for utilizing flow boiling heat transfer in microchannels. Most of researches focused on the flow instability investigation in a single or multiple microchannel(s) with fixed hydraulic diameter. The effect of channel size on flow instability in a single microchannel is quite limited.

- Flow orientation studies on flow instability in microchannels are rarely involved. More fundamental investigations need to be conducted to provide experimental observations to extend MEMS design and applications in future.

- So far, most studies were carried in straight channel(s). Studies on curved channel study can be of interest due to the development of secondary flows in the channel.

- All the listed previous research works were conducted by applying uniform heat fluxes. Non-uniform heat flux study in a single or multiple microchannel(s) is quite limited. However, this kind of operating conditions is more closed to the reality. The flow boiling heat transfer, the flow instability or the flow patterns may be very different to uniform heated cases.

- Inlet orifices in horizontal microchannel(s) have been studied and proven its ability to control or eliminate the flow instability. However, the effect of an inlet orifice in vertical flow directions still has to be investigated.

The objectives of this study are,
- To study the flow oscillation types and features at the onset of flow instability (OFI) in a single vertical microtube.

24

- To investigate the effect of hydraulic diameter on flow instability in a single vertical microtube.

- To study the effect of flow orientation on the flow instability in a single microtube.

- To understand the sensitivity of the operating conditions (the mass flux and the heat flux) on the flow boiling instability as the hydraulic diameter decreases in different flow orientations.

- To test the ability of inlet orifice on the flow instability controlling in a vertical single microtube.

Chapter 3

3 Experimental Methodology

3.1 Facility

Figure 3.1 illustrates the experimental facility. It is comprised of a closed working flow loop, a degassing branch and a set of data acquisition system. During the flow instability experiments, the dielectric liquid FC-72 (3M Company – Appendix A) as the working fluid is driven by a magnetically coupled gear pump (Cole-Parmer, 75211-22) which has a maximum flow volume rate 250 ml/min and a maximum power 517 kPa (75 psi). Then, FC-72 passes a 15 μm filter (Swagelok, SS-4TF-15) which is used to remove small impurities before FC-72 enters the system. Three rotameters (Omega, FL-1463-S/FL-1445-G/FL-1446-S) with different measurement ranges are used to monitor and measure a flow volume rate. After passing a rotameter, the subcooled working flow enters the test section, a single microtube, vertically (either vertical upward or vertical downward). The DC power supply (BK Precision, 1665) provides heat fluxes uniformly on the microtube surface. T-type thermocouples (Omega, TQSS-116G-6) and pressure transducers (Omega, PX01C1-075GV/PX02C1-050GV) are placed at both ends of the microtube to collect
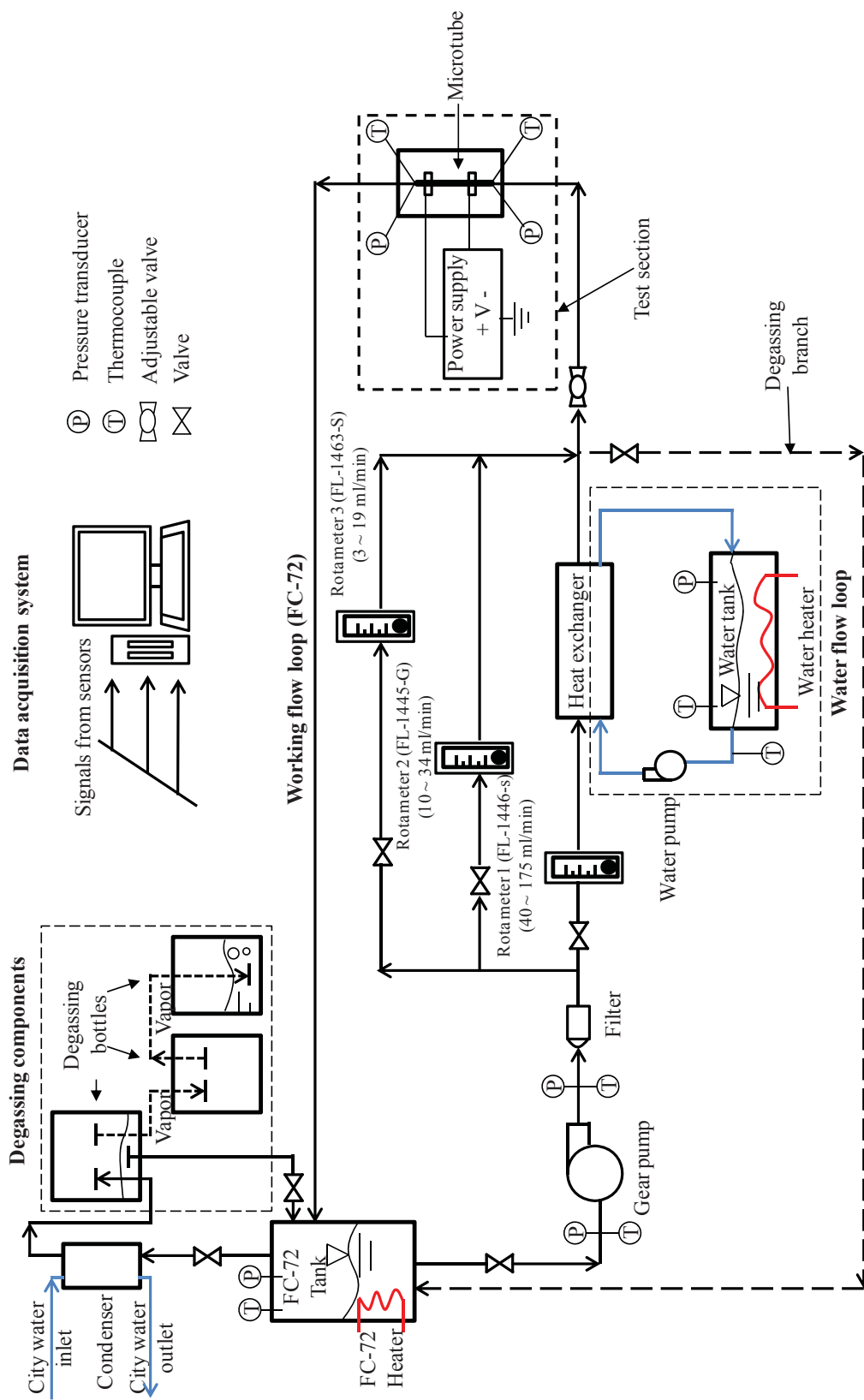
Figure 3.1: The schematic of the experimental facility

experimental data, which are recorded by the data acquisition system (National Instruments). Then, the working fluid goes back to the FC-72 tank. During the degassing, FC-72 is preheated by a 1 kW heater (Tempco, TSP02244) which is installed inside the FC-72. After passing the filter and the rotameter, FC-72 is sequentially heated to a desired temperature in a coiled copper heat exchanger to be able to vaporize. The vapor then returns to the FC-72 tank, the condenser (Spirec, S1TG1208) condenses FC-72 vapor. The separated air is discharged by the degassing components. The procedures of degassing will be introduced in Section 3.3. This facility is similar to the one used and validated by Fan (2013).

3.2   Test Section

The test section is fixed on a customized vertical board, as shown in Figure 3.2. The drawings of the customized components are attached in Appendix B. An example of the test section package in the vertical upward flow orientation is illustrated in Figure 3.3 (a). A separator is installed at the channel outlet to separate liquid and vapor in order to prevent vapor accumulation. The downward test section is identical to the upward one except the flow orientation and the separator's location. For convenience, in the rest of this thesis, VU represents the vertical upward flow orientation/configuration; VD represents the vertical downward flow orientation/configuration.

Three sizes of stainless steel microtubes (McMaster Carr) with identical length are selected to be investigated in the current study. The geometric parameters of these microtubes are listed in Table 3.1. The alternative names, Tube L (large), Tube M (medium) and Tube S (small), are used for distinguishing them in the rest of this thesis.
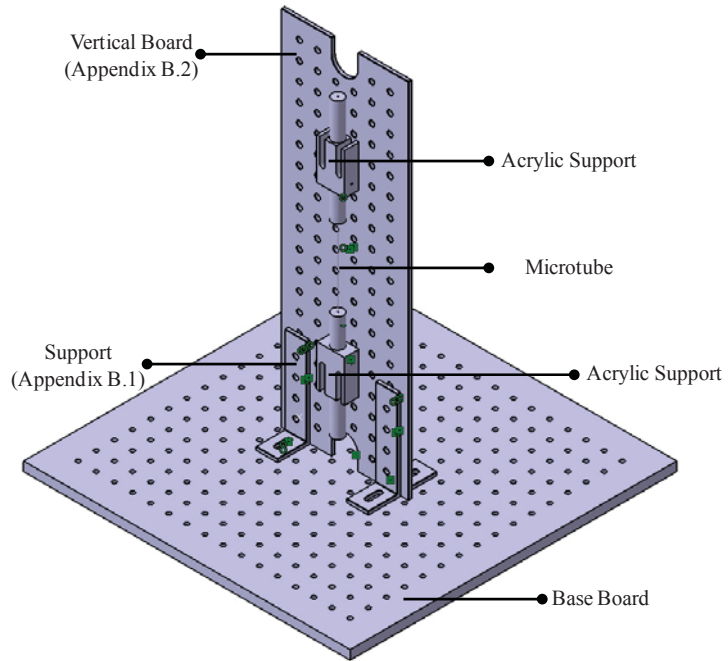
(a)
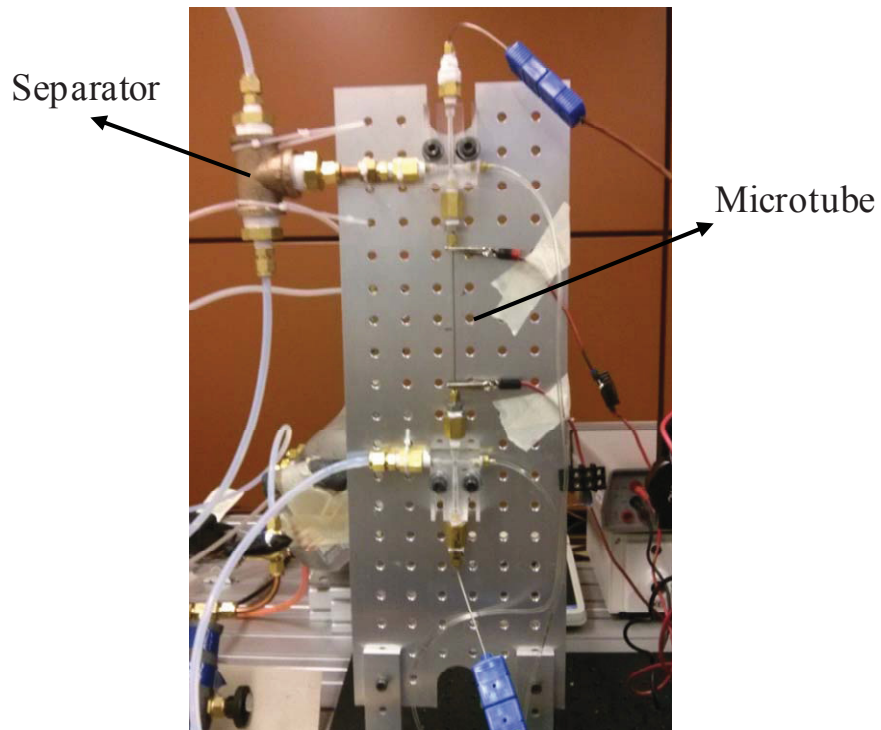
(b)

Figure 3.2: The test section installation (a) the schematic drawing (not to scale) (b) the

real test section

For the specific investigations dealing with the effect of the inlet orifice on the control of flow instability, the test section had to be modified. Tube L is selected as the main microtube, whose hydraulic diameter is presented by D_h. For Tube L, two smaller microtubes with different hydraulic diameters are used (Table 3.2). Their area ratios are 50% and 20% (Eq. (3.1)).

$$Area\ ratio\ \%\ (AR\%) = \frac{A_o}{A} \times 100\% = \frac{D_o^2}{D_h^2} \times 100\% \qquad (3.1)$$

Figure 3.3 (b) is an example of a 10 mm length inlet orifice attached to Tube L. There is a 5 mm overlapped length between both tubes and sealed by J.B. Glue. Before experiments, the leakage tests are performed to insure the adhesive quality.

Table 3.1: The geometric parameters of three microtubes

Parameters	Tube L	Tube M	Tube S
Hydraulic Diameter D_h (mm)	0.889	0.533	0.305
Length L (mm)	125	125	125
Heated Length L_h (mm)	100	100	100

Table 3.2: The geometric parameters in the inlet orifice effect investigation

Inlet Orifice Effect	Without Orifice	50% Inlet Orifice	20% Inlet Orifice
Microtube (Tube L) D_h (mm)	0.889	0.889	0.889
Inlet orifice D_o (mm)	--	0.635	0.406
Area ratio % (D_o^2/D_h^2)	100	51	21
Microtube length L (mm)	125	125	125
Microtube heated length L_h (mm)	100	100	100
Inlet orifice length L_o (mm)	--	10	10
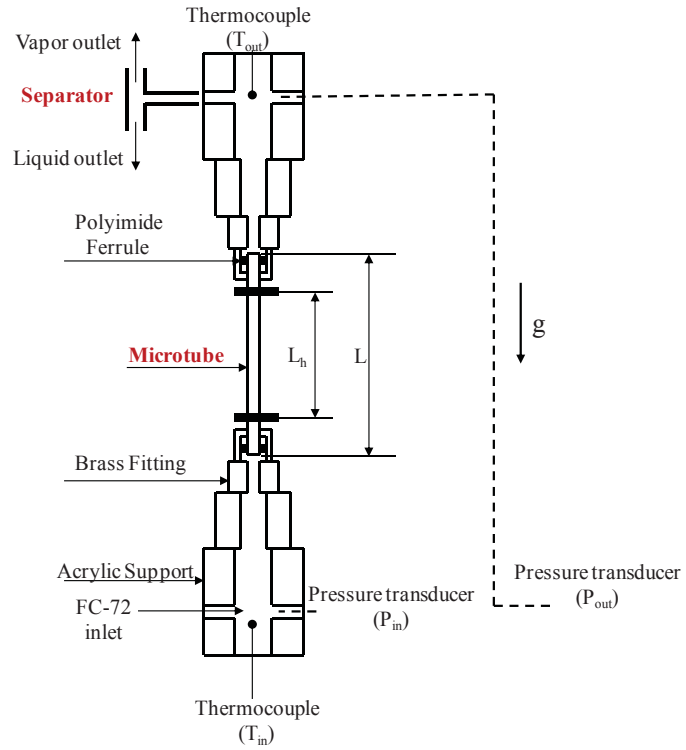
(a)
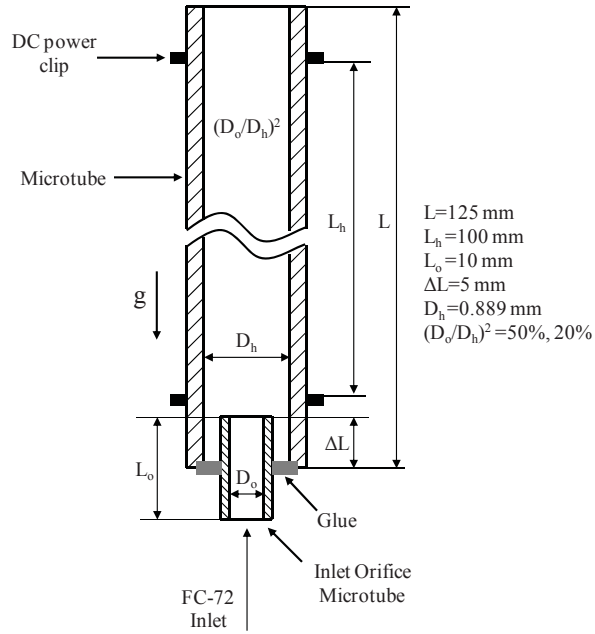
(b)

Figure 3.3: (a) The schematic of vertical upward configuration (b) The schematic of microtube with an inlet orifice (not to scale)

3.3 Experimental Methods and Test Matrix

3.3.1 Degassing

Since FC-72 has a highly air solubility (near 50% in volume), degassing is a must-have step before any experiments. The concept of degassing is to vaporize FC-72, and then condense FC-72 vapor – air mixture. The FC-72 vapor is condensed to its liquid phase and the air is separated and discharged. Because the facility contains several branches, the degassing has to be performed by circulating FC-72 vapor through each branch. Moreover, in order to protect the gear pump (the maximum operating temperature is 40 °C, in Figure 3.1), the vaporization has to be accomplished after the gear pump. Therefore, a water heat exchanger is introduced to induce the vaporization. The degassing procedure is briefly listed below.

1. Before degassing, all valves in the degassing branch have to be opened, and keep other branches closed.

2. Both FC-72 and the water are preheated at the same time, but with different heating rates. For the current facility, it is recommended that when the water temperature in the tank is increased to 40 °C, FC-72 temperature in tank is better around 54 °C.

3. After the water temperature in its tank reaches 40 °C, the water pump can be turned on to circulate the hot water through the heat exchanger.

4. Simultaneously, the cooling water loop of condenser can be circulated, and then the condenser can be turned on. The gear pump can be run to circulate preheated FC-72 through the system at a flow rate of 60 ml/min. As the preheated FC-72 passes the copper heat exchanger, it will be heated continuously.

5. The inlet temperatures of the gear pump (no more than 40 °C) and the water pump (no more than 80 °C) has to be monitored during degassing. Usually, the vaporization can be observed when the inlet temperature of the water pump is around 65 °C.

6. Once the vaporization occurs, the facility keeps running about 10 minutes, and all branches should be degassed one by one. Simultaneously, all temperature limitations should be monitored. The heater powers can be adjusted if necessary to protect the facility.

7. After 10 minutes, both FC-72 and water heaters should be turned off. Then, the condenser and the water pump are turned off. Only the gear pump is kept running to cool down FC-72 for a while.

8. Last, all components should be shut down, and all valves should be locked.

The whole degassing process may last around one hour. After FC-72 in the tank is back to room temperature, the experiment can be conducted.

3.3.2   Onset of Flow Instability Detection

The OFIs as real-time pressure and temperature fluctuations are captured in both vertical flow orientations. More specifically, during the experiment, a desired mass flux is fixed and then a heat flux is applied uniformly on the tube surface in small increments until the fluctuations occurred. Since some initial fluctuations, typically lasting between 10 to 20 minutes, might be caused by the operation, the fluctuations due to OFIs are considered those sustaining more than 30 minutes (Fan, 2013). After reaching such conditions, the temperature and the pressure at both ends of the test section are recorded in 5-minute

sampling time span at 400 Hz sampling frequency in order to describe OFI characteristics. Otherwise, the heat flux is continuously increased until the sustained fluctuations are detected. However, in some cases, no sustained and characterized flow oscillations can be detected at all operating conditions, for example in Tube S, the transient point is observed instead. The details will be discussed later. Pressure measurements are used to quantitatively analyze the oscillation features in terms of dominant frequencies (see Appendix C), amplitudes and the magnitude of fluctuations which can be calculated by Eq. (3.2) and Eq. (3.3), respectively.

$$MAG = \frac{1}{N}\sum x_i \qquad (3.2)$$

$$AMP = \text{maximum}\{x_i\} - MAG \qquad (3.3)$$

3.3.3 Test Matrix

During all measurements, the inlet temperature is maintained around 24 °C. The test matrix in current experiment is listed in Table 3.3.

Table 3.3: Test matrix

Parameters	Conditions
Flow directions	Vertical upward (VU), Vertical downward (VD)
Subcooled inlet temperature, T_{in}	24 °C
Outlet pressure, P_{out}	10 kPa (VU), 6 kPa (VD)
Heat flux, q"	1.8 – 9.6 W/cm^2
Mass flux, G	700 – 1600 kg/m^2·s

3.4   Uncertainty Analysis

The flow volume rates are measured by rotameters (Omega, FL-1463-S/FL-1445-G/FL-1446-S) with different measurement ranges (Figure 3.1). Two thermocoumples (Omega, TQSS-116G-6) and two pressure transducers (Omega, PX01C1-075GV/PX02C1-050GV) are used to measure the temperature and the pressure at both ends of the microtube. Since the microtube is directly exposed to air, the heat loss induced has to be estimated. In this study, we followed the method of Fan (2013) (see Appendix D). The facility and the calculation uncertainties are listed in Table 3.4. The uncertainties of measured parameters are obtained from user manuals or by direct measurement. The calculated uncertainties of inlet orifice area ratio, pressure drop, mass flux and heat flux are based on the method provided by Moffat (1988) (Eq. (3.4) − (3.7)). The uncertainty calculations are demonstrated in Appendix E.

$$\delta AR\% = \sqrt{\left(\delta D_o \frac{\partial AR\%}{\partial D_o} \right)^2 + \left(\delta D_h \frac{\partial AR\%}{\partial D_h} \right)^2} \tag{3.4}$$

$$\delta \Delta P = \sqrt{\left(\delta P_{in} \right)^2 + \left(\delta P_{out} \right)^2} \tag{3.5}$$

$$\delta G = \sqrt{\left(\delta T \frac{\partial G}{\partial T} \right)^2 + \left(\delta Q \frac{\partial G}{\partial Q} \right)^2 + \left(\delta D_h \frac{\partial G}{\partial D_h} \right)^2} \tag{3.6}$$

$$\delta q'' = \sqrt{\left(\delta V \frac{\partial q''}{\partial V} \right)^2 + \left(\delta I \frac{\partial q''}{\partial I} \right)^2 + \left(\delta D_h \frac{\partial q''}{\partial D_h} \right)^2 + \left(\delta L_h \frac{\partial q''}{\partial L_h} \right)^2} \tag{3.7}$$

Table 3.4: Uncertainties

Measured Parameters	Sources	Uncertainty, δ
T-type thermocouples, T	Omega	$\pm$ 0.5 °C
Rotameter 1 (FL-1446-S), Q	Omega, 5% of full scale	$\pm$ 8.75 ml/min
Rotameter 2 (FL-1445-G), Q	Omega, 5% of full scale	$\pm$ 1.70 ml/min
Rotameter 3 (FL-1463-S), Q	Omega, 5% of full scale	$\pm$ 0.95 ml/min
Inlet Pressure Transducer, P_{in}	Omega, 0.05% of full scale	$\pm$ 0.259 kPa
Outlet Pressure Transducer, P_{out}	Omega, 0.05% of full scale	$\pm$ 0.173 kPa
Voltage, V	BK Precision 1665	$\pm$ 0.05 V
Current, I	BK Precision 1665	$\pm$ 0.05 A
Tube hydraulic diameter, D_h, D_o	McMaster Carr	$\pm$ 0.0127 mm
Heated length, L_h	Direct measurement	$\pm$ 1 mm
Calculated Parameters	**Equations**	**Uncertainty, δ**
50% AR inlet orifice	(3.4)	$\pm$ 2.5%
20% AR inlet orifice	(3.4)	$\pm$ 1.4%
Pressure drop, ΔP	(3.5)	$\pm$ 0.311 kPa
Mass flux (Rotameter 2), G	(3.6)	$\pm$ 6%
Mass flux (Rotameter 3), G	(3.6)	$\pm$ 6%
Heat flux, q"	(3.7)	$\pm$ 0.11 – 0.25 W/cm^2

Chapter 4

4   Flow Instability in Various Hydraulic Diameters

Figure 4.1 shows the flow stability regimes of three microtubes in VU. For Tube L and M, the onsets of flow instability (OFIs) are determined for mass fluxes between 700 and 1600 kg/m^2·s. A flow is stable at any operating condition below the OFIs; otherwise, it becomes unstable. For Tube S, only the transient points are observed instead. A transient point represents a stable flow rapidly turning to another stable state. There is some regularity that can be noticed on Figure 4.1. First, at a given mass flux, the OFI/transient point occurs earlier in a smaller hydraulic diameter microtube. Second, in larger hydraulic diameters, OFI usually occurs, and an increased mass flux can help to delay its occurrence. However, in smaller ones, a transient point is more often observed, and a large mass flux cannot show significant effect on the transient point appearance. The details will be discussed in the following sections.
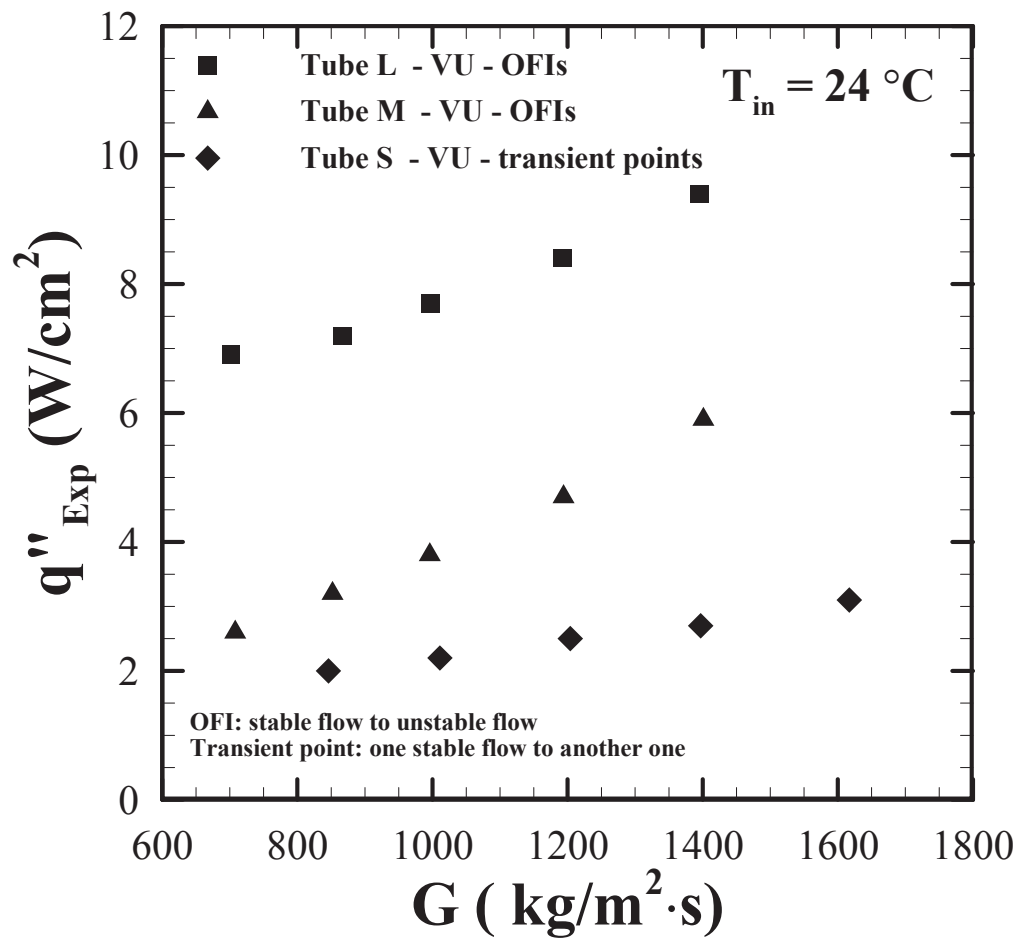
Figure 4.1: The map of flow stability regimes in three microtubes in VU

4.1 Flow Characteristics in Different Hydraulic Diameters

In this section, the points in Figure 4.1 at the mass flux of 1000 kg/m^2·s are selected for the hydraulic diameter effect investigation. The corresponding real-time flow fluctuations are presented, compared and discussed.

Figure 4.2 (a) and (b) illustrates the real-time flow oscillations at the OFI in Tube L in terms of pressure and temperature fluctuations. The heat flux at the OFI is q"$_{OFI,Tube\ L}$ = 7.7 W/cm^2. The inlet pressure experiences high frequency oscillations superimposed on the peak of low frequency oscillations, as shown in Figure 4.2 (a). *Low frequency oscillation* is called Pressure Drop Oscillation (PDO), which is normally induced by static Ledinegg instability. As the working flow passes the heated microtube, the onset of nucleate bubble appears when enough heat flux is applied. At a certain vapor quality, the pumping power is not sufficient to maintain the flow rate due to the increased internal pressure demand. Then, the flow rate suddenly drops to a lower value which can be observed by naked eyes from the rotameter in current experiment. Ledinegg instability occurs. Because of the reduced mass flux, the high local temperature field leads to bubble growth. When the growing bubble reaches the tube wall, it is confined and expands towards both upstream and downstream directions. Hence, a reversed flow is formed, that is, PDO is triggered. Boure et al. (1973) noted that this type of oscillations had features of a low frequency (about 0.1 Hz) and large amplitudes. It occurred when a compressible volume was formed at upstream of, or within, the heated section. In microchannel studies, Qu and Mudawar (2003) explained that a compressible volume might be caused by a significant amount of vapor generation once the heat flux exceeded the incipient boiling value. *High frequency oscillations* which are superimposed on the peak of PDOs have the
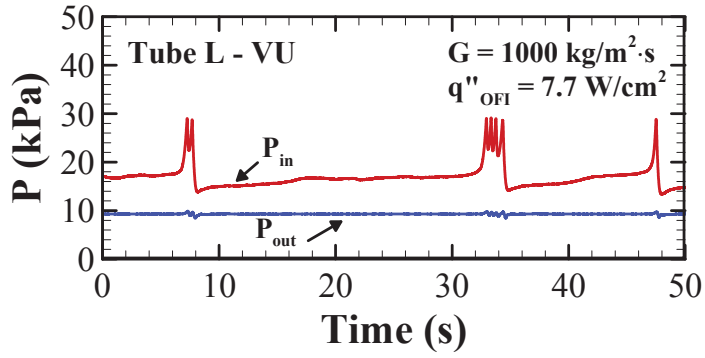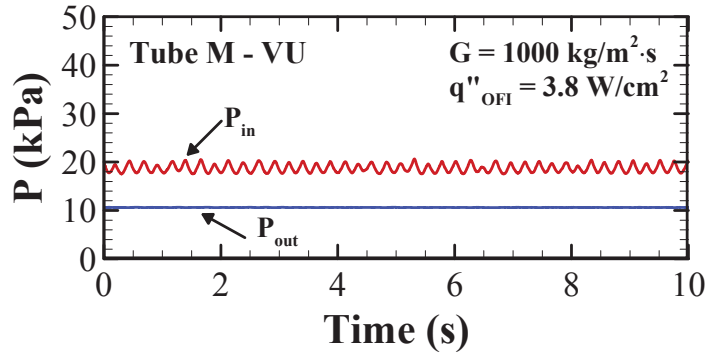
(a)
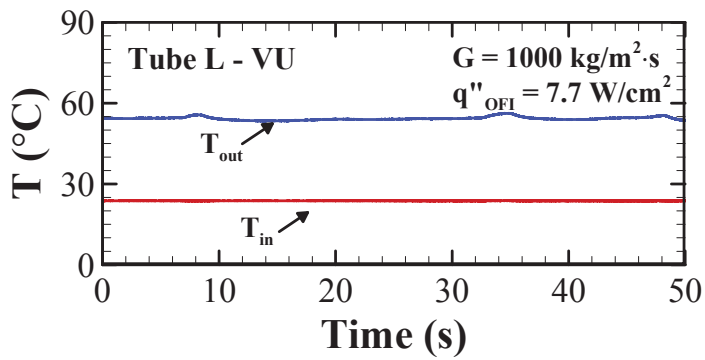
(b)
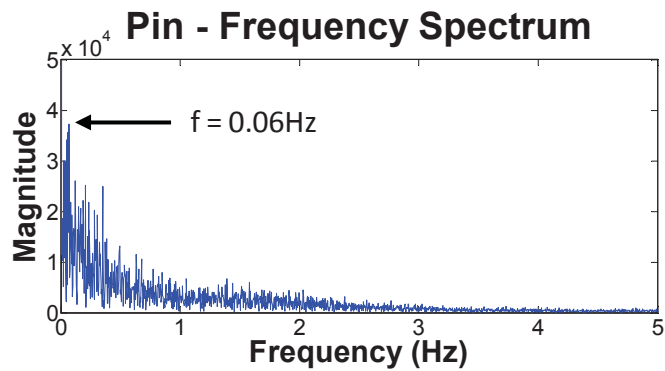
(c)

Figure 4.2: The real-time of flow oscillations in terms of (a) pressure, (b) temperature and

(c) the inlet pressure frequency spectrum in Tube L in VU at the mass flux of 1000

kg/m^2·s

characteristics of Density Wave Oscillation (DWO). Since an elongated bubble formed at the channel upstream reduces the mass flux, the fellow bubbles grow up quickly. The slug flow consisting of large vapors and liquid slugs may appear. Because of the density differences between liquid and vapor, the working flow experiences high and low densities alternatively when travelling along the channel, so DWOs with a comparatively high frequency (usually about 1 Hz, Boure et al., 1973) and small amplitude appear. When the confined vapor core is close to the channel outlet, it can easily leave the tube because of low outlet pressure. Hence, the reduced mass flux can rapidly go back to its original level. More subcooled liquid is imported into the tube again so that an oscillation cycle repeats. In summary, in the current case, the Ledinegg instability causes PDOs and DWOs, which may correspond to a slug flow and a bubbly flow alternatively switching. In Figure 4.2 (b), the outlet temperature also fluctuates in phase with the pressure oscillations between saturated and subcooled values. Figure 4.2 (c) plots the frequency spectrum of inlet pressure oscillations during 5-minute. The major frequency is about $f_{OFI,Tube\ L} = 0.06$ Hz which has the strongest power spectral density (magnitude). This value indicates PDOs are more dominant during the flow oscillations. The amplitude of the pressure fluctuations is $AMP_{OFI,Tube\ L} = 12.7$ kPa which implies PDOs are dominant.

As the hydraulic diameter is reduced (Tube M), the inlet pressure oscillation type becomes pure DWO at the OFI, as shown in Figure 4.3 (a). The OFI occurs at a lower heat flux $q"_{OFI,Tube\ M} = 3.8$ W/cm^2. Unlike in Tube L, a small amount of heat flux can easily cause the bubble confinement in Tube M, and expands rapidly along the tube length. A strong and sustained slug flow then may be formed leading to pure DWOs. Yin et al. (2014) compared the growth rate before and after bubble confinement in a

41

singlerectangular microchannel via flow visualization. They observed that the growth rate after bubble confinement was significantly increased than before confinement. Their finding evidenced that once a bubble is confined, the flow pattern would turn to the slug flow containing quickly a large amount of vapor. In the current study, the outlet temperature in Tube M (Figure 4.3 (b)) stays at saturated level during flow oscillations, which possibly corresponds to the slug flow which is containing saturated vapor and liquid slugs. The large value of dominant frequency ($f_{OFI,Tube\ M}$ = 4.6 Hz) in Figure 4.3 (c) also reflects DWOs dominate the flow oscillations.

As the hydraulic diameter further reduces to Tube S (Figure 4.4), a transient point is observed at $q"_{tran,Tube\ S}$ = 2.2 W/cm^2. The transient point represents the change of a stable flow to a new stable state. Therefore, its real-time pressure and temperature display very small oscillations, and no characterized frequency can be determined. The corresponding phenomenon is that as the flow boiling starts, the bubble confinement is immediately triggered. The outlet temperature suddenly drops a little bit due to the reduction in flow rate. At the same time, the inlet pressure increases with a small amount and starts fluctuating with tiny amplitudes. In a few seconds, the outlet temperature reaches a saturated level and maintains at that value. The inlet pressure keeps sustained tiny oscillations. Brutin et al. (2003) classified steady and unsteady states in their flow boiling instability investigation in multiple microchannels. The authors defined that the steady state had low fluctuation amplitudes (< 1 kPa) and no characteristic oscillation frequency. The unsteady state had high amplitudes (> 1 kPa) and a characteristic oscillation frequency. Hence, in the current study, the flow condition is considered to switch to another stable flow rapidly; for example, a single-phase liquid suddenly turns to an

(a)
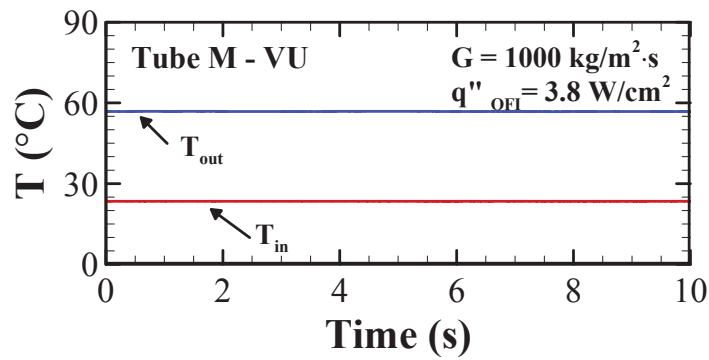
(b)
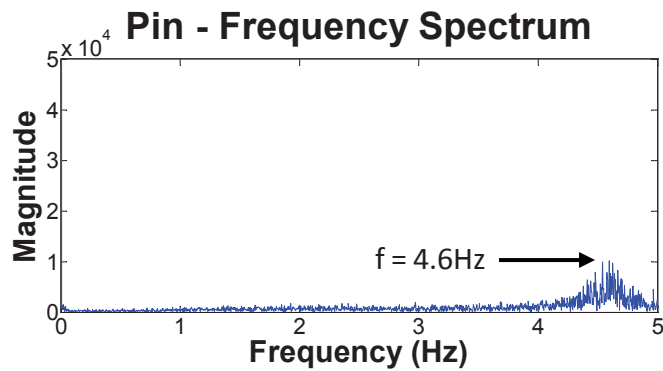
(c)

Figure 4.3: The real-time of flow oscillations in terms of (a) pressure, (b) temperature and

(c) the inlet pressure frequency spectrum in Tube M in VU at the mass flux of 1000
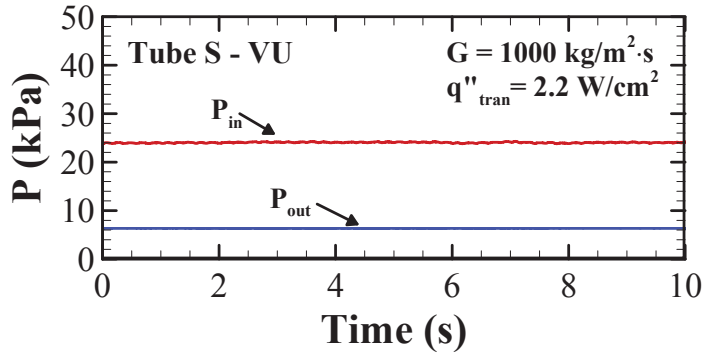
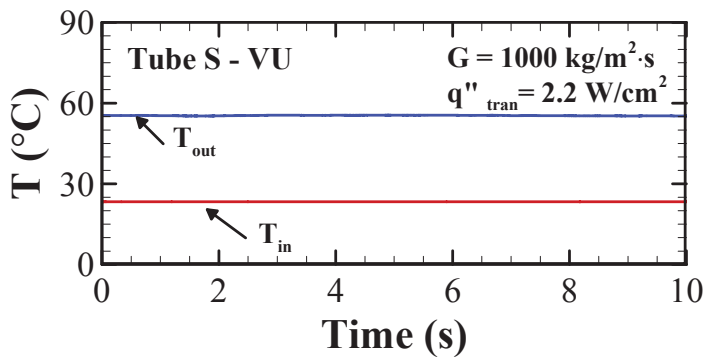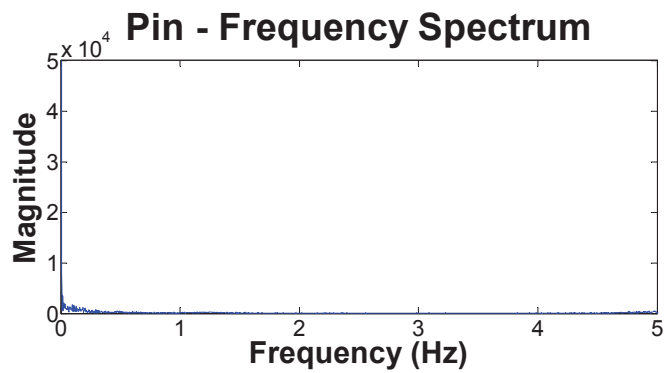kg/m^2·s

(a)

(b)

(c)

Figure 4.4: The real-time of flow oscillations in terms of (a) pressure, (b) temperature and (c) the inlet pressure frequency spectrum in Tube S in VU at the mass flux of 1000 kg/m^2·s

annular flow due to the early bubble confinement once the bubble nucleation starts at low heat flux. Harirchian and Garimella (2009) noted that the incipience heat flux (when boiling occurs) decreases as the channel size decreased. Moreover, the slug flow and intermittent churn/annular flow were most often observed in a small channel. The bubbly flow and intermittent churn/wispy-annular flow usually existed in a large channel. Their observations are similar to the results and assumptions in current study.

4.2 Effect of Mass Flux and Heat Flux on Flow Instability

4.2.1 Effect of Mass Flux

In this section, the flow oscillation types and features at OFIs/transient points at two mass fluxes of 850 kg/m^2·s and 1200 kg/m^2·s (Figure 4.1) in each microtube are exhibited and compared.

Figure 4.5 plots the real-time flow oscillations of OFIs in Tube L at different mass fluxes. At the mass flux of 850 kg/m^2·s (Figure 4.5 (a)), the heat flux at OFI is q"$_{\text{Tube L,850}}$ = 7.2 W/cm^2, and the dominant flow oscillation type is DWO. The saturated outlet temperature and a high dominant frequency f$_{\text{Tube L,850}}$ = 0.67 Hz match the features of DWOs. As the mass flux increased (Figure 4.5 (b)), a new OFI occurs when a higher heat flux is applied (q"$_{\text{Tube L,1200}}$ = 8.4W/cm^2), and its dominant flow oscillation type changes to PDO with a low frequency f$_{\text{Tube L,1200}}$ = 0.037 Hz. Namely, DWOs become weaker. The outlet temperature fluctuates between saturated and subcooled values. A large drag force induced by a large mass flux is probably the reason for postponing the OFI occurrence and restrict DWOs. Since bubble departure diameters become smaller as the drag force increases, the flow pattern is dominated by bubbly flow with small volume of vapor.
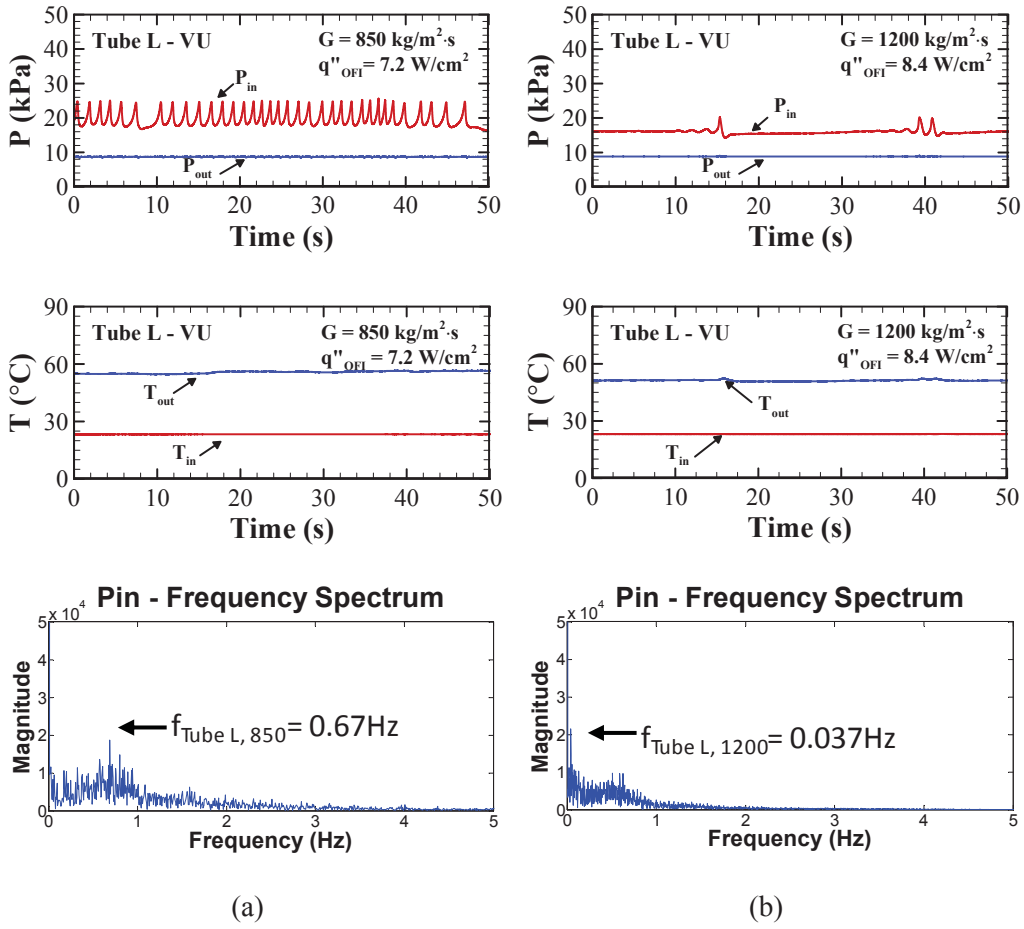
45

Figure 4.5: The real-time of flow oscillations in Tube L in VU at the mass flux of (a) 850 kg/m^2·s and (b) 1200 kg/m^2·s

Therefore, more heat flux is required to trigger flow oscillations at a large mass flux. Bogojevic et al. (2013) mentioned in their study that the bubble departure diameters decreased with the mass flux increasing. Wang et al. (1994) also noticed that in conventional size channels, DWOs could be controlled by increasing the mass flux because it limited the vapor quality.

Figure 4.7 (a) gives the real-time flow oscillations in Tube M at the mass flux of 850 kg/m^2·s. The pure DWOs dominating flow oscillations occurs when the heat flux q"$_{Tube}$ $_{M,850}$ = 3.2 W/cm^2 is applied. The dominated frequency and amplitude of flow oscillations are f$_{Tube M,850}$ = 4.1 Hz and AMP$_{Tube M,850}$ = 2.14 kPa. When the mass flux is increased to 1200kg/m^2·s (Figure 4.7 (b)), OFI occurrence is delayed (q"$_{Tube M,850}$ = 4.7 W/cm^2). The flow oscillations are also dominated by pure DWOs. As discussed before, an increased drag force can reduce bubble departure diameters. Therefore, more heat flux is needed to trigger OFI. Moreover, in Tube M, the early bubble confinement can cause the flow pattern to quickly change to a strong slug flow even at a larger mass flux. Unlike in Tube L, the increased mass flux doesn't affect the flow oscillation types but changes the flow oscillation characteristics in Tube M (f$_{Tube M,1200}$ = 5.1 Hz and AMP$_{Tube M,1200}$ = 1.93 kPa).

Figure 4.6 exhibits the mass flux effect in Tube S. At the mass flux of 850 kg/m^2·s (Figure 4.6 (a)), a transient point occurs when a small heat flux is applied (q"$_{Tube S,850}$ = 2.0 W/cm^2). The real-time pressure and temperature are quite stable. After the mass flux increased to 1200 kg/m^2·s (Figure 4.6 (b)), the transient point occurs at a higher heat flux(q"$_{Tube S,1200}$ = 2.5 W/cm^2). However, the increment of heat flux is not remarkable. Although a large drag force can reduce bubble departure diameters, the bubble can be easily confined in a small hydraulic diameter once the bubble nucleation happens. In

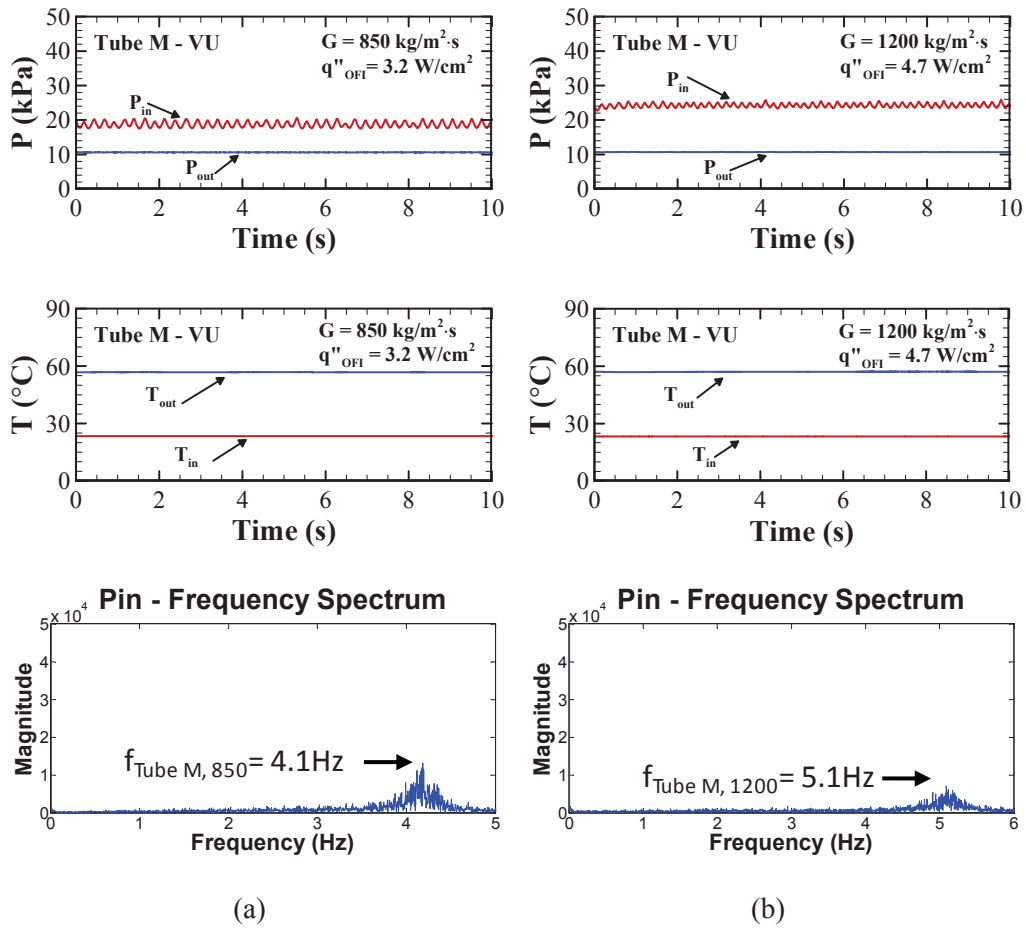Figure 4.6: The real-time of flow oscillations in Tube M in VU at the mass flux of (a) 850 kg/m^2·s and (b) 1200 kg/m^2·s
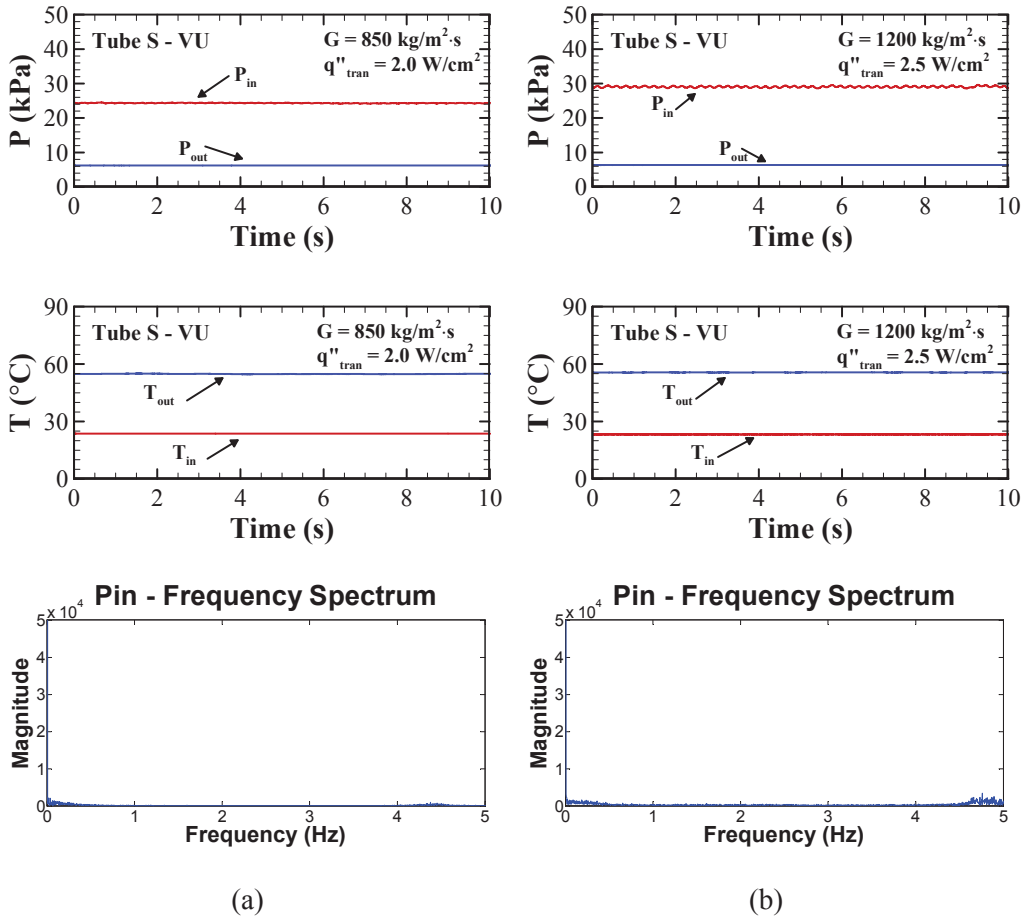
Figure 4.7: The real-time of flow oscillations in Tube S in VU at the mass flux of (a) 850 kg/m^2·s and (b) 1200 kg/m^2·s

other words, in Tube S, the increased mass flux can neither delay a transient point occurrence effectively nor changing flow characteristics, but the average of pressure drop is increased ($MAG_{Tube\ S,\ 850} < MAG_{Tube\ S,\ 1200}$) as the mass flux increases.

Figure 4.8 plots the flow oscillation features of each OFI point in Figure 4.1. In general, the increased mass flux in Tube L can postpone OFIs appearance. It can also change flow oscillation types and features ((a) f, (b) AMP and (c) MAG) of OFIs, but their changing trends are dependent on flow patterns rather than mass fluxes. The increased mass flux in Tube M can also delay OFI appearance but cannot affect flow oscillation types and features; however, the average pressure drop is increased as the mass flux increases. The effect of mass flux on transient point occurrence and flow behaviors in Tube S can be negligible.

4.2.2 Effect of Heat Flux on Flow Instability

In Tube L, the effect of heat flux on flow instability at OFIs is investigated. In Figure 4.9 (a), the real-time flow oscillations of the OFI at the mass flux of 700 kg/m^2·s are presented. The flow oscillation type is a compound type, including Ledinegg, PDOs and DWOs instabilities. The dominant frequency is f_{OFI} = 0.022 Hz. After increasing the heat flux to q" = 8.3 W/cm^2 (Figure 4.9 (b)), the dominant frequency is increased and its amplitude is decreased. These changings indicate that at a fixed mass flux, DWOs are more dynamic as the heat flux increases. This can be explained by the fact that when a mass flux is fixed, more power input not only leads to more bubbles nucleation at the channel upstream section but also extends the nucleation site towards the channel downstream sections. Tibirica and Ribatski (2014) performed a flow visualization to investigate bubble characteristics during flow boiling in a single horizontal microtube
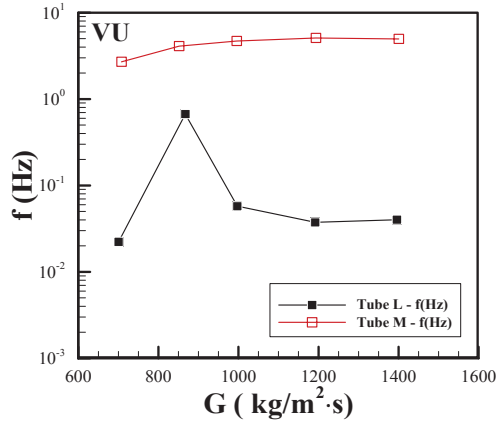
(a)
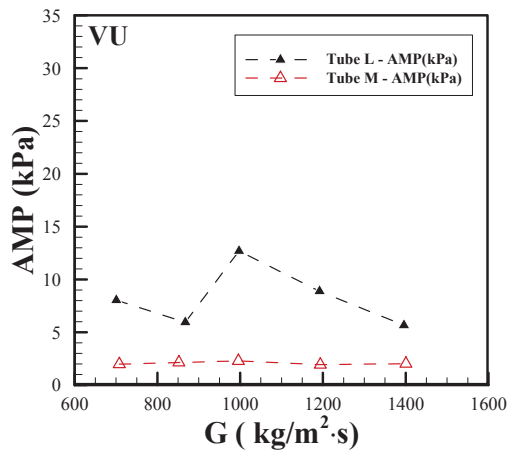
(b)
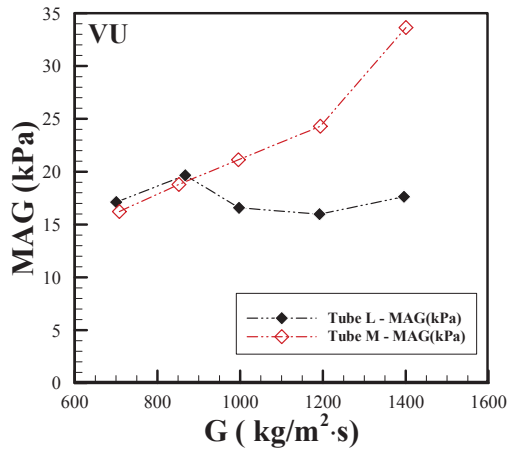
(c)

Figure 4.8: Comparison of the flow oscillation characteristics Tube L and M in VU (a) f,

(b) AMP and (c) MAG

with 0.400 mm hydraulic diameter. They observed that at a constant mass flux, when more heat flux is applied more bubble nucleation sites were activated. Therefore, in this study, a strong confined bubble/slug may cause more active DWOs. This observation is also similar to the findings of Fan and Hassan (2012) for a single horizontal microtube. As more heat flux are added (Figure 4.9 (c)), DWO features are more active. The dominant frequency becomes higher, and the amplitude becomes smaller. Another example of the heat flux effect in Tube L at the mass flux of 1000 kg/m^2·s is presented in Figure 4.10. At the OFI as shown in Figure 4.10 (a), PDO is the dominant flow oscillation type, while DWO type is less observed. With more heat flux added (Figure 4.10 (b) and (c)), DWOs become more intensive as well. For Tube M and S, the effect of heat flux has not been investigated. It is because based on the results in Tube L, it is expected that more heat flux applied in Tube M may enhance DWOs as well, but may cause local dryout in Tube S since the liquid film of the annular flow may become thinner.

4.3 Summary

The flow oscillation types and characteristics in three identical length microtubes with different hydraulic diameters ($D_{h, \text{Tube L}}$ = 0.889 mm, $D_{h, \text{Tube M}}$ = 0.533 mm and $D_{h, \text{Tube S}}$ = 0.305 mm) have been studied and compared for a mass flux range from 700 to 1600 kg/m^2·s in VU. In Tube L, OFIs with compound flow oscillation types, including Ledinegg, PDOs and DWOs, have been always observed. However, the dominant type and characteristics (f, AMP and MAG) depended on flow patterns rather than mass fluxes When PDO dominated flow oscillations, the outlet temperature oscillated between subcooled and saturated values, which might suggest that an intermittent flow pattern
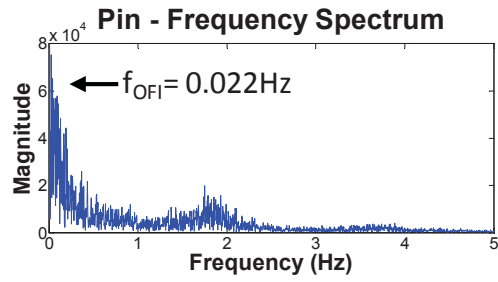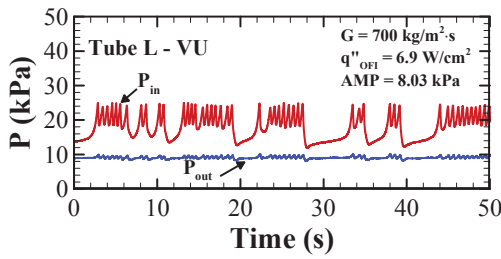
(a)
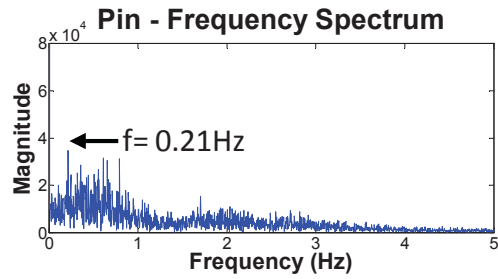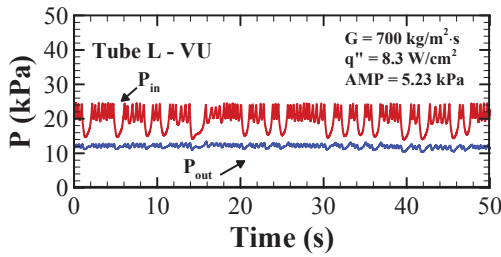
(b)
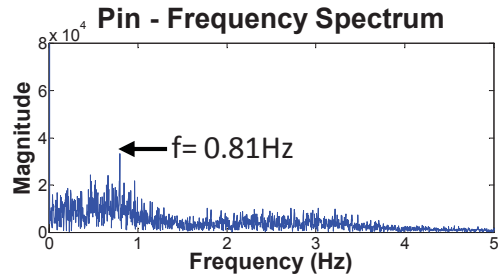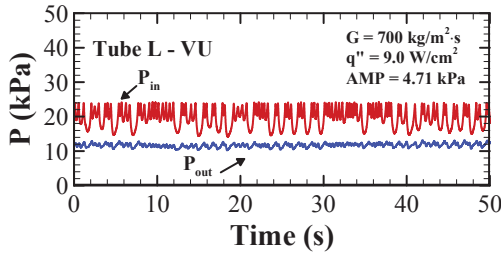
(c)

Figure 4.9: The real-time of flow oscillations in Tube L in VU at the mass flux of 700

kg/m^2·s (a) at the OFI and (b) (c) after the OFI

53
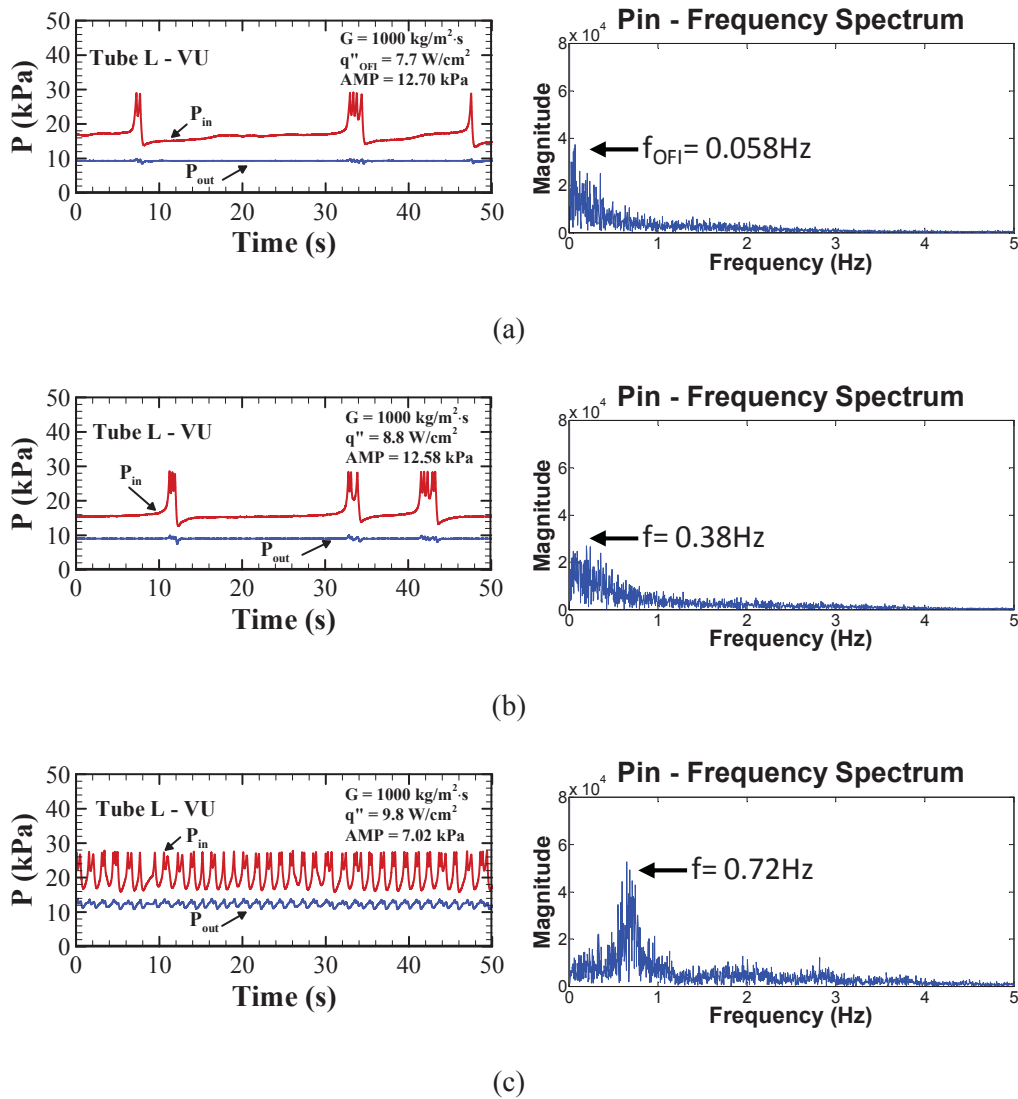
Figure 4.10: The real-time of flow oscillations in Tube L in VU at the mass flux of 1000 kg/m^2·s (a) at the OFI and (b) (c) after the OFI

existed. When DWO dominated, the outlet temperature was almost maintained at the saturated level, which might suggest that a slug flow dominated the flow pattern. The increased mass flux could suppress DWO and postpone OFI occurrence; however, the increased heat flux could intensify DWO. In Tube M, OFIs with pure DWOs have always been detected earlier than in the case of Tube L for the same mass flux. The possible flow pattern might be a slug flow. The flow oscillation characteristics varied with the mass flux. The increased mass flux could weaken DWOs but increases the magnitude (MAG) of flow oscillations and delay OFI occurrence. In Tube S, the transient points were only observed instead of OFIs. They appeared earlier than in the other two larger microtubes. This might be explained by the fact he bubble were confined before departure and rapidly formed a stable annular flow. The transient point occurrence and characteristics were less sensitive to the increase in mass flux.

Chapter 5

5 Effect of Flow Orientation on Flow Instability

In this chapter, the effects of flow orientation on flow instability are investigated. Figure 5.1 provides a map of flow stability regimes in three microtubes in both vertical flow directions (VU and VD). In Tube L, OFIs are observed in both flow directions. In Tube M, OFIs are recorded in VU, but only transient points are detected in VD. In Tube S, transient points are always observed in VU; however, in VD, the flow blockage phenomenon appears. The flow orientation affects OFI/transient point occurrence. As the hydraulic diameter reduces, this effect is weakening but brings dryout in VD. The details will be discussed in next sections.

5.1 Comparison of Flow Oscillation Features in Both Flow Orientations

5.1.1 In Tube L

In Figure 5.2, the real-time flow oscillations of OFI in Tube L in VD at the mass flux of 850 kg/m^2·s are illustrated. PDOs dominated flow oscillations (Figure 5.2 (a)) occur at a heat flux of q"$_{OFI, VD}$ = 7.1 W/cm^2 which is earlier than that in VU (q"$_{OFI, VU}$ = 7.7 W/cm^2).
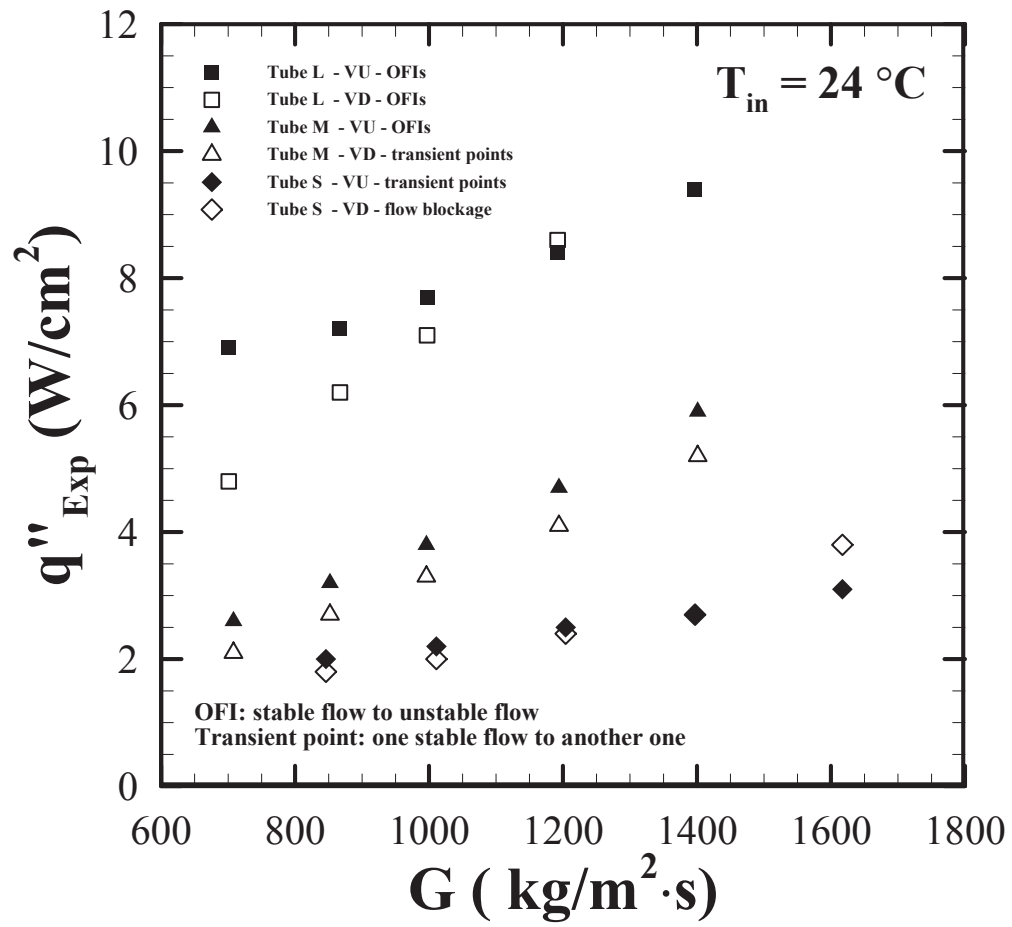
Figure 5.1: The map of flow stability regimes in three microtubes in VU and VD

Since the flow orientation is the only variable in the current experiment, the buoyancy force is considered as the main reason causing the differences in OFI occurrence. In VU, as previously discussed, the bubbly flow and elongated/slug flow alternatively switching may correspond to complex flow oscillations. In VD, because the buoyancy force acts on bubbles against the flow direction, the bubbles are difficult to be exhausted and rather accumulated and coalesced each other; that is, the reversed flow can be formed with less heat flux input. Once the elongated/confined bubble is discharged, single-phase liquid is quickly imported. Because of the obstruction due to the buoyancy force, another large vapor forming and discharging requires more time. Hence, the flow oscillations in VD have a lower frequency ($f_{VD,Tube\ L} = 0.02$ Hz $< f_{VU,Tube\ L} = 0.06$ Hz). Zhang et al. (2005) also observed a similar finding in VD in multiple microchannles. Their flow qualitative visualization results showed that all sizes of bubbles moving towards the channel downstream were slower than the bulk liquid due to the buoyancy force.

As the mass flux is increased to 1200 kg/m^2·s (Figure 5.3), a new OFI appears in VD at a heat flux almost similar to the case in VU ($q"_{OFI,\ VD} = 8.6$ W/cm^2 $\approx q"_{OFI,VU} = 8.4$ W/cm^2). However, the corresponding flow oscillations last only for a short time (about 3 minutes) with large amplitudes ($AMP_{VD} = 17.0$kPa $> AMP_{VU} = 8.9$ kPa) and a low frequency ($f_{VD} = 0.020$ Hz $> f_{VU} = 0.037$ Hz). A large drag force may reduce the bubble departure diameters so that more heat flux is required to trigger more nucleation sites. However, the buoyancy force suppresses bubbles traveling to the channel downstream, so small bubbles coalesce together to form a compressible volume gradually leading to the flow oscillations with large amplitudes. After several oscillations, the confined bubbles are more and more difficult to be discharged. They are accumulated in the channel and
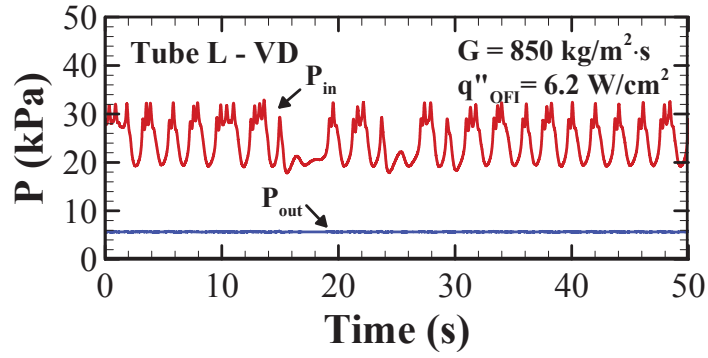
(a)
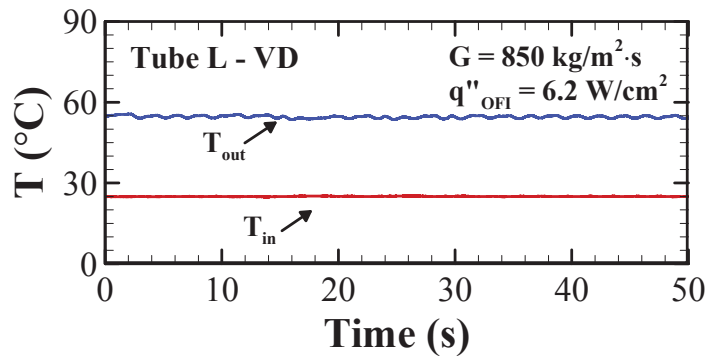
(b)
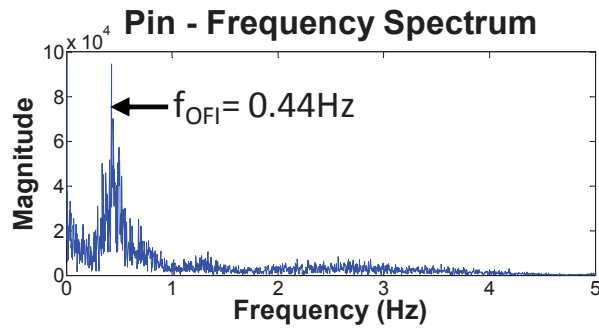
(c)

Figure 5.2: The real-time of flow oscillations in terms of (a) pressure, (b) temperature and

(c) the inlet pressure frequency spectrum in Tube L in VD at the mass flux of 850

kg/m^2·s

(a)

(b)

(c)

Figure 5.3: The real-time of flow oscillations in terms of (a) pressure, (b) temperature and

(c) the inlet pressure frequency spectrum in Tube L in VD at the mass flux of 1200

kg/m^2·s

then may cause the flow pattern turning to a stable annular flow. This phenomenon implies that a large mass flux in VD can delay OFI occurrence or even leading to a restable flow. The buoyancy force suppresses the bubble discharging inducing early dryout, however.

Figure 5.4 lists the heat flux effect on flow instability in VD in Tube L at the mass flux of 700 kg/m^2·s. When the OFI is observed (Figure 5.4 (a)), the flow oscillations are combined, including Ledinegg instability, PDOs and DWOs. The dominant frequency ($f_{OFI,VD}$ = 0.24 Hz) indicates PDO is the major oscillation type. As the heat flux is increased (Figure 5.4 (b)), the flow oscillation type becomes pure DWO with a small amplitude and a high dominant frequency (f = 4.2 Hz). After applying more heat flux (Figure 5.4 (c)), the flow oscillations tend to re-stablize. The amplitudes of flow oscillations are decreased and no major characteristic frequency can be observed. In VU, as previously discussed, an increased heat flux enhances DWOs. Contrarily, in VD, more heat flux triggers more nucleation sites, and the buoyancy force suppresses bubble discharging. The bubbles are gradually accumulated and then may cause the flow pattern changes to be the stable annular flow rapidly. Therefore, more heat flux causes the flow oscillations to re-stabilize in VD.

5.1.2   In Tube M

For Tube M, in VD (Figure 5.5) at the mass flux of 850 kg/m^2·s, only the transient point is detected. Its occurrence is earlier than the OFI occurrence in VU ($q"_{VD,Tube M}$ = 3.3 W/cm^2 < $q"_{VU,Tube M}$ = 3.8 W/cm^2). The trapped bubbles due to the buoyancy force grow up or coalesce to form annular flow in a short period of time. Hence, once the heat flux reaches a certain level, a stable flow rapidly changes to another stable state without

61
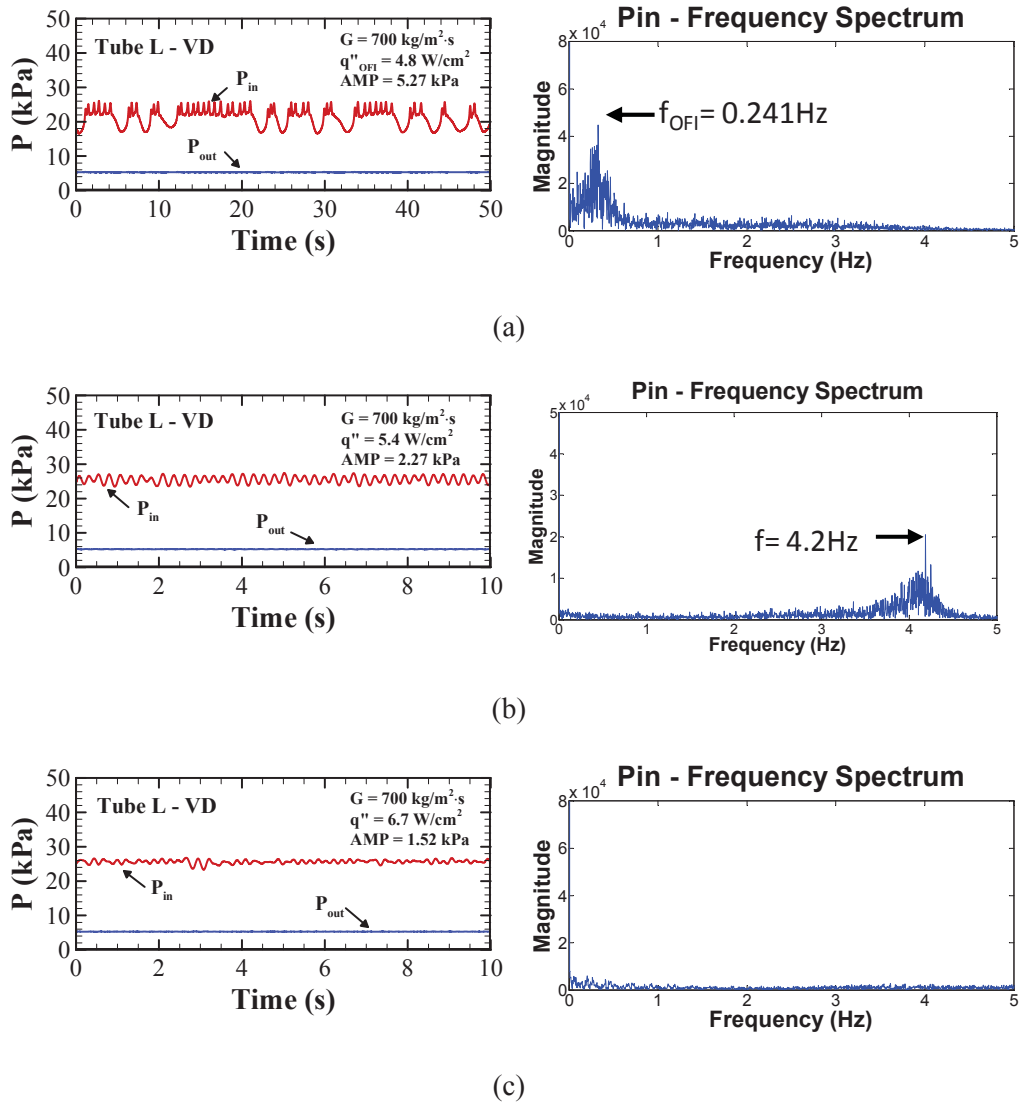
Figure 5.4: The real-time of flow oscillations in Tube L in VD at the mass flux of 700 kg/m²·s (a) at the OFI and (b) (c) after the OFI
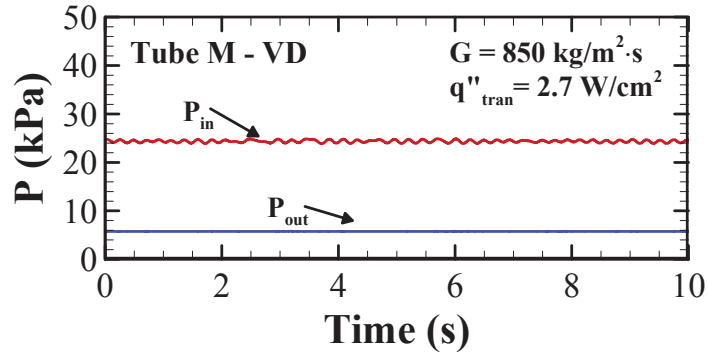
(a)
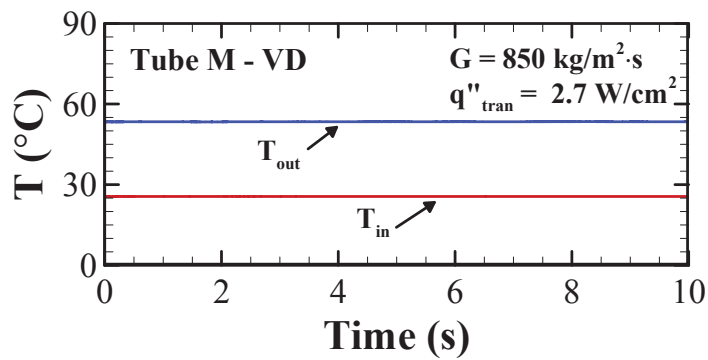
(b)
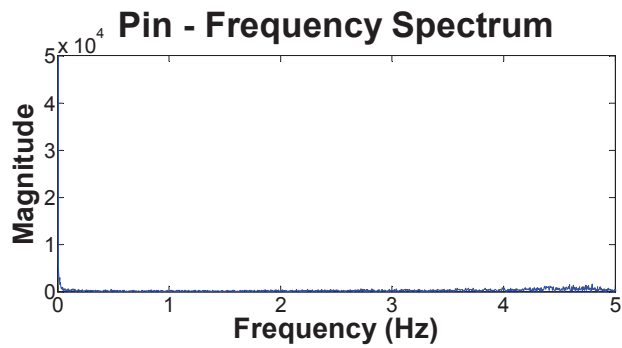
(c)

Figure 5.5: The real-time of flow oscillations in terms of (a) pressure, (b) temperature and (c) the inlet pressure frequency spectrum in Tube M in VD at the mass flux of 850 kg/m^2·s

experiencing sustained and intensive oscillations.

As the mass flux is increased to 1200 kg/m^2·s (Figure 5.6), a transient point is still observed, but postponed. In Tube M in VU, as previously discussed, pure DWOs dominant OFIs are always detected. Their occurrence can be delayed by a large mass flux. In VD, only transient points are recorded, and an increased mass flux also can postpone the transient point appearance.

5.1.3   In Tube S

For Tube S, in VD, the flow blockage phenomenon is observed. For example, at the mass flux of 850 kg/m^2·s in VU (Figure 5.1), the transient point occurs at $q"_{VU,Tube\ S} = 2.2$ W/cm^2. In VD, the mass flux suddenly drops to zero at a similar heat flux ($q"_{VD,Tube\ S} = 2.0$ W/cm^2); and the flow is completely restricted. No liquid can be observed at the outlet, some tiny bubbles are floating out from the inlet, instead of. Even an increased mass flux cannot break through this flow blockage. In order to protect the system, the experiment is ceased so that no real-time data are recorded. The flow blockage is considered caused by the buoyancy force and the early confinement. Qi et al. (2007) had a similar observation in their flow boiling investigations in a single microtube but using liquid nitrogen. They reported the block phenomenon at the onset of nucleate boiling since the bubble discharge rate was lower than the bulk flow rate. Besides, the authors pointed that both block phenomenon and the Critical Heat Flux (CHF) led to dryout but the triggering conditions were different. The former was caused by vapor blocking the flow, and the later was caused by dryout of liquid film. In the current study, even at higher mass fluxes, the flow blockage always appears in VD in Tube S and cannot be postponed effectively. Hence, it can be noticed that an increased mass flux cannot show effective influences
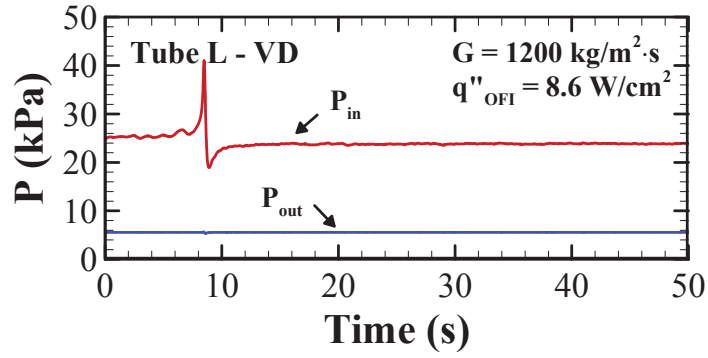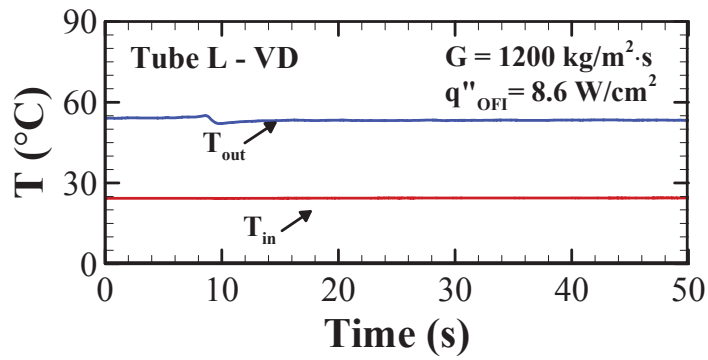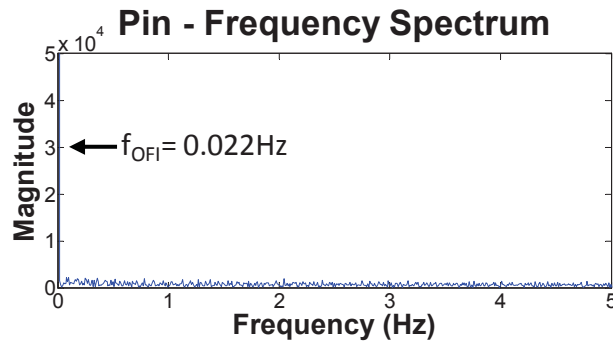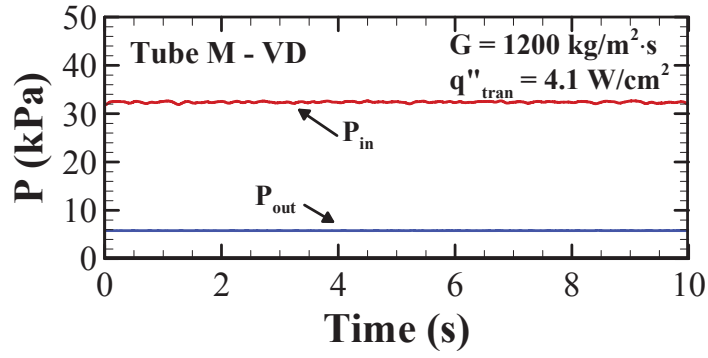
(a)
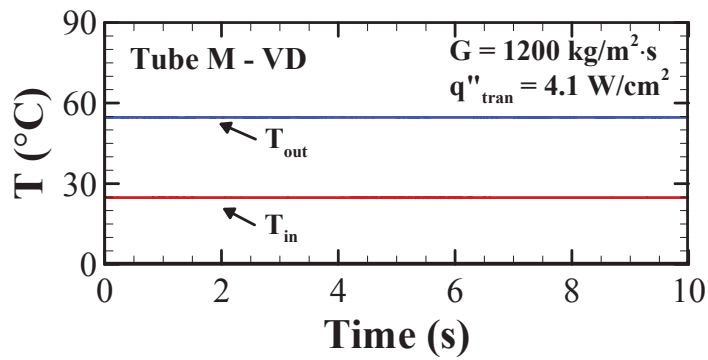
(b)
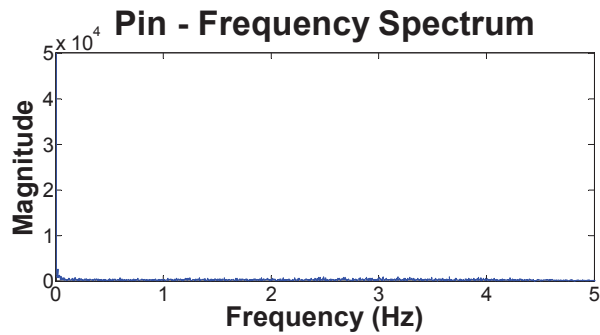
(c)

Figure 5.6: The real-time of flow oscillations in terms of (a) pressure, (b) temperature and (c) the inlet pressure frequency spectrum in Tube M in VD at the mass flux of 1200 kg/m^2·s

either to delay the flow blockage or to break through after the flow blockage happened.

Figure 5.7 provides an overview of flow oscillation features between VU and VD in Tube L and M. To sum up, in Tube L (Figure 5.7 (a)), a large mass flux can postpone OFIs occurrence and changes flow oscillation characteristics as well in both vertical flow orientation. However, the magnitude of flow oscillations in VD is always larger than in VU due to the difficulty in bubble discharging. In Tube M (Figure 5.7 (b)), OFIs are recorded in VU, but transient points are often observed in VD. An increased mass flux can delay OFI/transient point occurrence and cause the pressure drop increasing in both flow directions. In Tube S, the boiling flow may be blocked in VD.

5.2   Effect of Inlet Orifice on Flow Instability Control

As previously introduced, a reversed flow due to rapid bubble bidirectional expansion is believed to cause the flow instability. A suitable solution is to increase the inlet pressure to suppress the reversed flow. In the current study, two sizes of inlet orifices are investigated on the flow instability control in both vertical flow orientations.

After installing an inlet orifice on Tube L, the operating conditions without inlet orifices are applied to verify the ability of inlet orifice to control flow oscillations. At the mass flux of 700 kg/m^2·s, in VU (Figure 5.8 (a)), with 50% inlet orifice, when the operating conditions are similar to the no-orifice case, an OFI still occurs; however, the flow oscillation type is static Ledinegg oscillation. In VD (Figure 5.8 (b)), the flow oscillations are eliminated. However, the inlet pressure is $MAG_{50\%} = 19.12$ kPa, which is lower than the average inlet pressure with no-inlet orifice ($MAG_{OFI} = 21.04$ kPa), which was not observed in VU. It may be explained by the difference in flow behavior at the
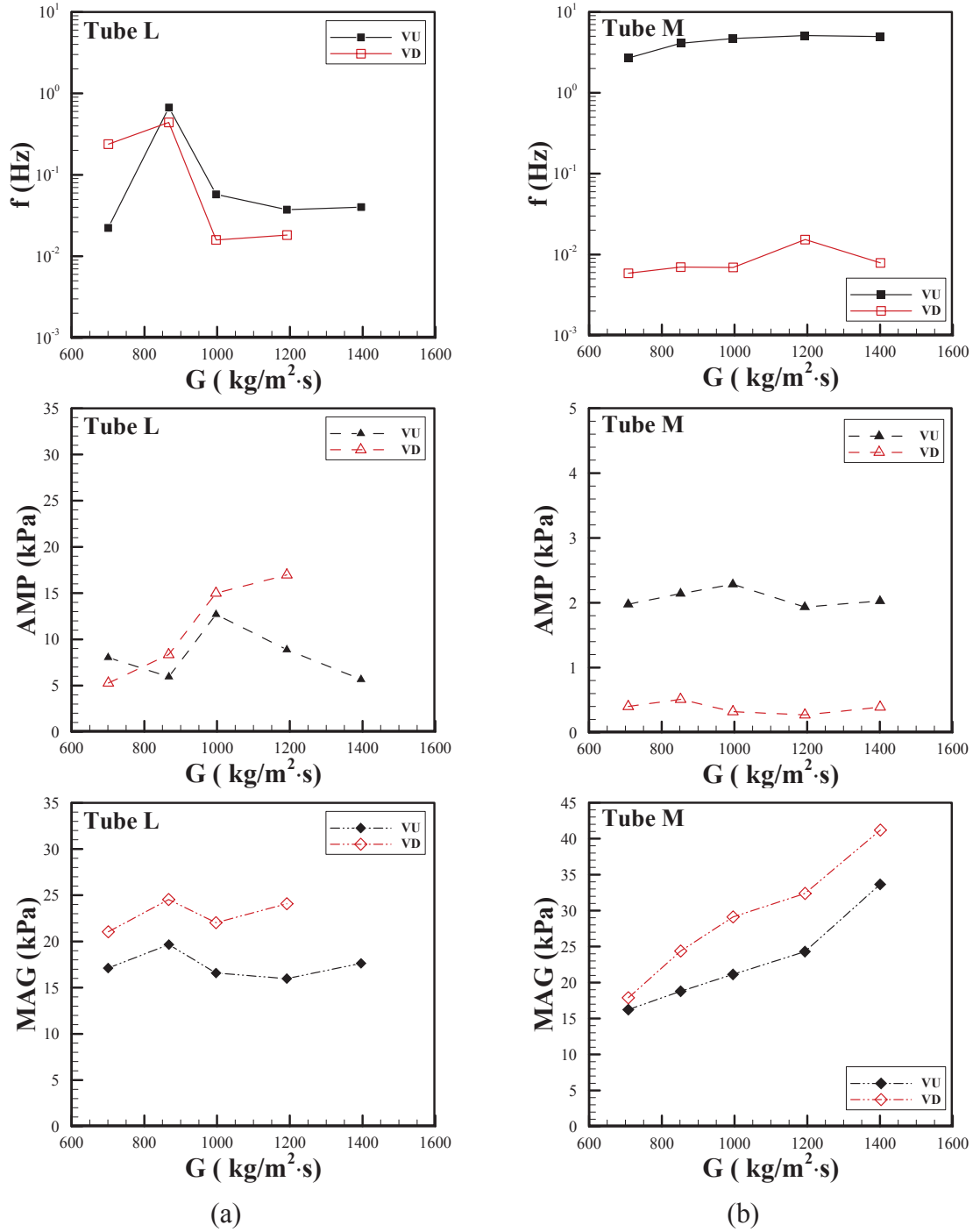
Figure 5.7: Comparison of the flow oscillation characteristics (f-AMP-MAG) in VU and VD in (a) Tube L and (b) Tube M
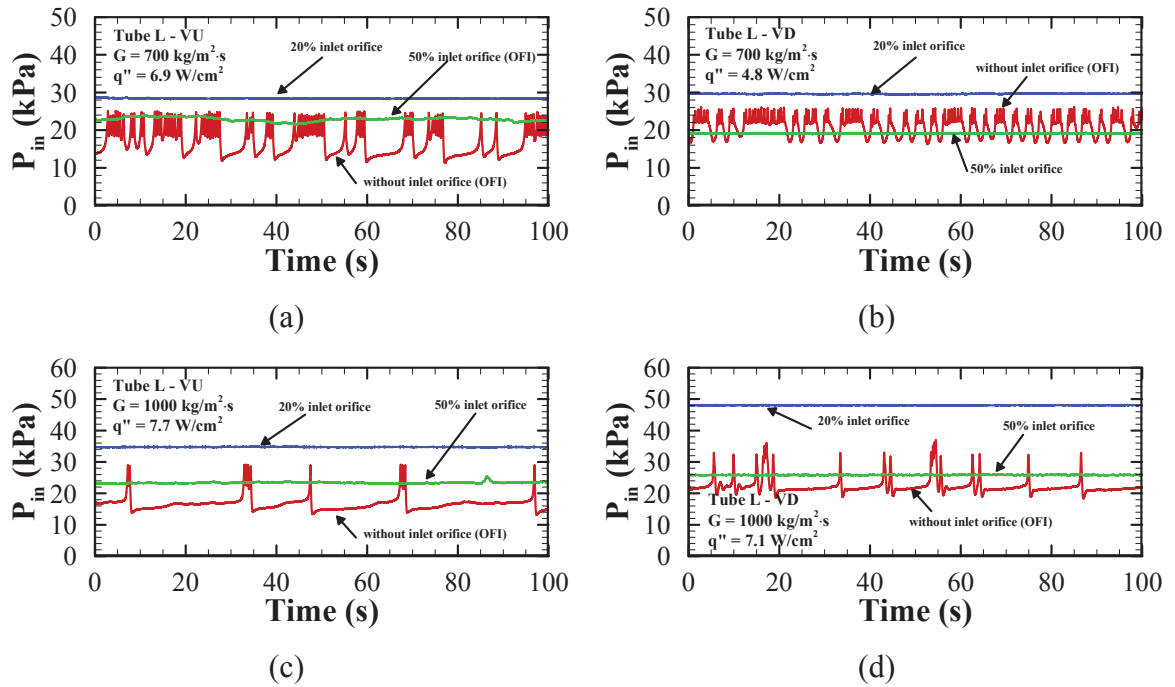
Figure 5.8: The real-time flow behaviors with an inlet orifice at the operating conditions when the OFIs occur without an inlet orifice: (a) G = 700 kg/m²·s in VU, (b) G = 700 kg/m²·s in VD, (c) G = 1000 kg/m²·s in VU and (d) G = 1000 kg/m²·s in VD

inlet orifice due to the flow orientation. Park et al. (2009) and Schneider et al. (2007) found that the inlet jet stream and the flashing effect due to the inlet orifice in a horizontal microchannel heat sink might affect flow behavior. At the mass flux of 1000 kg/m^2·s, in VU (Figure 5.8 (c)), with 50% inlet orifice, the OFI cannot be detected at the same heat flux applied in no-orifice case. The magnitude of the inlet pressure with 50% inlet orifice (MAG$_{50\%}$ = 27.23 kPa) are higher than the magnitude of the inlet pressure in no-orifice cases (MAG$_{OFI}$ = 16.58 kPa), but smaller than its maximum. Fan and Hassan (2012) concluded that as an inlet orifice was applied in a single horizontal microtube, if the inlet pressure was higher than the maximum value of flow oscillations without flow restriction, the inlet orifice was about to stabilize the flow. The difference between current study and the finding from Fan and Hassan (2012) may be caused by the vertical upward flow. In VD (Figure 5.8 (d)), when the operating condition is set as the OFI occurs without inlet orifice, the flow oscillations cannot be observed. The inlet pressure is MAG$_{50\%}$ = 25.86 kPa, which is higher than the average inlet pressure without inlet orifice (MAG$_{OFI}$ = 22.03 kPa). This observation is similar to the cases with VU. At both mass fluxes, with 20% inlet orifice, the flow oscillations are eliminated and no OFIs are observed in both vertical flow orientations.

The experiments to detect the OFIs with an inlet orifice are carried out in Tube L. With 50% inlet orifice, due to its large area ratio, it has a limited ability to restrict the reversed flow; therefore, OFIs still occur. The inlet pressure oscillations at OFIs with 50% inlet orifice and no-orifice are compared in Figure 5.9. At the mass flux of 700 kg/m^2·s, in VU (Figure 5.9 (a)), the OFIs with and without 50% inlet orifice occur at the same mass flux however, the static Ledinegg oscillation is detected instead of the combined
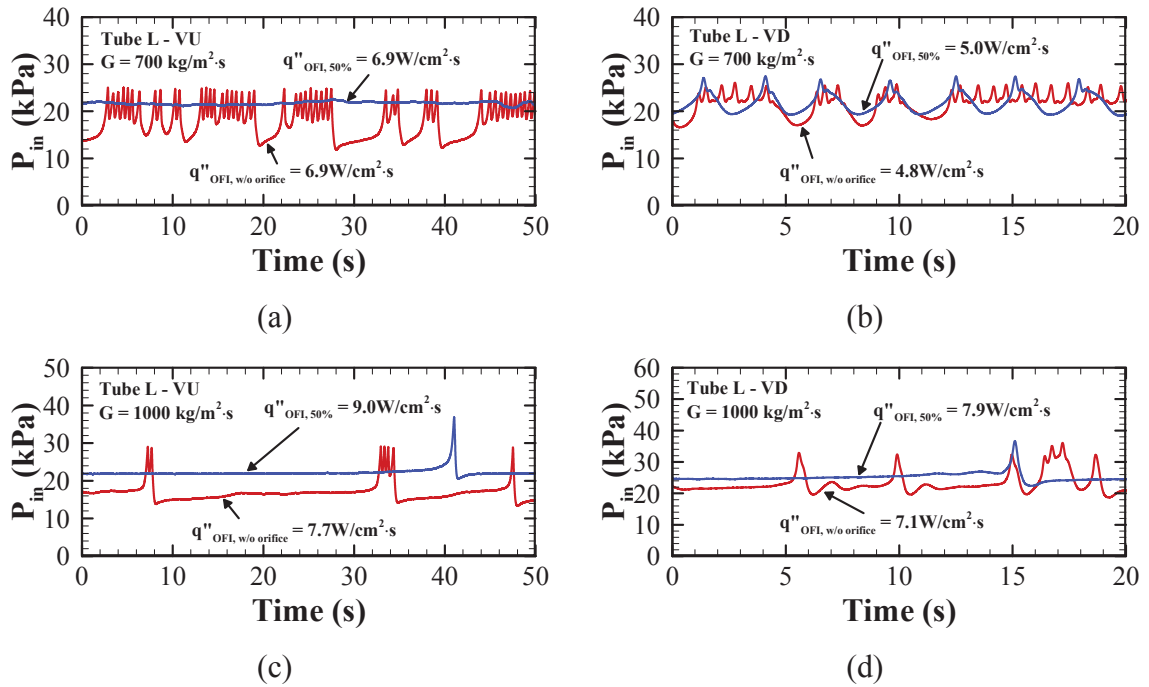
Figure 5.9: Comparison of the inlet pressure at OFIs with and without 50% inlet orifice in Tube L at the mass fluxes of (a) $G = 700$ kg/m^2·s in VU, (b) $G = 700$ kg/m^2·s in VD, (c) $G = 1000$ kg/m^2·s in VU and (d) $G = 1000$ kg/m^2·s in VD

oscillations when no inlet orifice applied. In VD (Figure 5.9 (b)), 50% inlet orifice can minimally delay the OFI occurrence; however, pure PDOs are still observed. The flow oscillations cannot be suppressed since inlet orifice area ratio is large. In addition, the buoyancy force aggravates the flow oscillations due to the bubble discharging difficulty. At the mass flux of 1000kg/m^2·s, in VU (Figure 5.9 (c)), 50% inlet orifice delays the OFI occurrence ($q"_{OFI, 50\%} > q"_{OFI, w/o \ orifice}$), and a low frequency pure PDO type dominates the flow oscillations instead of combined types when no-inlet orifice is applied. In VD (Figure 5.9 (d)), 50% inlet orifice delays the OFI occurrence as well but better than at a low mass flux. Hence, in the current investigations, 50% inlet orifice performance in VD is worse than in VU. 20% inlet orifice can eliminate the flow oscillations but increases the pressure drop simultaneously.

There are no experimental results of the effect of inlet orifice in Tube M and S. It is because based on the flow oscillation characteristics in both tubes observed previously, the inlet orifice is not applicable in both smaller tubes. In Tube M, without inlet orifice, pure DWOs were always observed due to early bubble confinement as discussed before. Since the inlet orifice is for suppressing the reversed flow which is the major source to cause PDOs, it is considered that may not control or eliminate pure DWOs in Tube M. In Tube S, without inlet orifice, only transient points were recorded without experiencing characteristic oscillations. Therefore, the inlet orifice is not required in Tube S.

5.3 Summary

The flow oscillation types and characteristics in VD have been investigated in three single microtubes, respectively. The results were compared to the cases in VU. The

buoyancy force effect was observed but caused different phenomena for different hydraulic diameters. In Tube L, the combined flow oscillations at the OFIs were recorded as in VU, but the magnitude of flow oscillations were always higher than in VU because the buoyancy force impeded the bubble discharge rate. At low mass fluxes, the OFI occurrence was early in VD. As the mass flux increased, the OFI occurrence in VD was closed to the cases in VU since the large drag force contributed to the bubble discharge. However, the increased heat flux turned the flow oscillations to re-stabilize in VD, which might imply the flow pattern changed to the stable annular flow. This phenomenon was not desired because more heat flux might cause local dryout. In Tube M, the transient points without characterized flow oscillation features have been observed in VD. The pressure drop increased as the mass flux increased and were always higher than in VU. In Tube S, the flow blockage was observed when small amount of heat flux was applied. Its appearance was not effectively affected by the mass flux. Moreover, the flow blockage was irreversible even increased mass flux after its appearance. This phenomenon was dangerous and would damage the system. The 50% inlet orifice could delay the OFI occurrence in Tube L in VD but worse than in VU. The 20% inlet orifice performance in VD was similar to the cases in VU but its pressure drop was higher than the cases in VU.

Chapter 6

6 Conclusion and Future Directions

6.1 Conclusion and Contributions

In this study, the flow instability types and characteristics in different hydraulic diameters of microtube in vertical upward and downward flow directions were experimentally investigated. Three sizes of stainless steel microtubes (D_h = 0.305, 0.533 and 0.889 mm) with identical heated length (L_h = 100mm) were tested. The subcooled coolant FC-72 was driven at the mass flux varying from 700 to 1600 kg/m^2·s, and the heat flux was uniformly applied on the tube surface from 1.8 to 9.6 W/cm^2. Two inlet orifices (the area ratios of 20% and 50%) were investigated on flow oscillation stabilization in vertical flow directions.

Ledinegg, PDO, DWO flow oscillation types were observed in a single vertical microtube. During combined oscillations (Ledinegg, PDOs and DWOs), the outlet temperature oscillated in phase with the inlet pressure between subcooled and saturated temperatures, and it implied that the intermittent flow pattern (the bubbly/slug flow alternatively switching) may have existed. During DWOs, the outlet temperature maintained at the saturated level, which might correspond to the slug flow. The OFI, the transient point and the flow blockage were observed depending on the hydraulic diameter,

the flow orientation and the operating conditions. The OFI, a threshold of characterized flow instability, most occurred in large hydraulic diameters or in VU. The transient point, the point where the flow changes from one stable state to another one once the bubble nucleation appears, usually appeared in small hydraulic diameters or in VD. The flow blockage was only observed in the smallest hydraulic diameter in VD. As the hydraulic diameter reduces, the OFI/transient point occurred earlier, and the combined flow oscillation type changed to pure DWO or re-stabilized. The buoyancy force effect on the OFI/transient point occurrence was decreased as the hydraulic diameter decreases, but it impeded the bubble discharging leading to flow blockage in a small hydraulic diameter in VD. The large drag force could delay OFI/transient appearance, but its ability reduced as the hydraulic diameter decreases. In a large tube or in VU, the flow oscillation range was usually wide. After flow started to oscillate, a considerable heat flux increment could make the flow re-stabilize. In a small tube or in VD, the flow oscillation range was comparatively narrow. A small amount of extra heat flux might lead to the re-stabilized flow or the dryout crisis after flow oscillations appeared. In current investigation, in the larger tube (Tube L), 50% inlet orifice performed better in controlling flow instability as the mass flux increases or in VU, and 20% inlet orifice can totally eliminate flow instability.

Hence, the combined and complex flow oscillations occurrence in large hydraulic diameters can be delayed by an increase in mass flux or controlled by adding an inlet orifice in vertical flow directions. As the hydraulic diameter decreases, the flow oscillations occur earlier and are not sensitive to the mass flux. The system with the vertical upward flow direction is better than the vertical downward one in terms of flow

74

instability since vertical downward configuration may bring early dryout crisis or flow blockage. It is recommended that, for future flow boiling microchannel heat sink design, moderate hydraulic diameter ($D_h > 0.500$ mm) with vertical upward flow is preferred.

6.2 Future Directions

Since the flow instability in microchannel(s) is complicated and affected by multiple parameters, comprehensive fundamental investigations are needed to be conducted in order to understand the nature of flow oscillations, the relationships between various parameters inducing flow instability and provide correlations and solutions for optimization designs. The follow studies can be carried on in the near future:

- The flow patterns at OFIs or transient points in different hydraulic diameters need to be visualized in order to observe the flow patterns changing trends. These observations can be useful for flow instability controlling investigations.

- The relationship among the flow instability, the heat transfer coefficient and the pressure drop needs to be studied fundamentally. Since as the hydraulic diameter reduces, the heat transfer may be enhanced, but the flow instability may occur at a low heat flux. The results are valuable for microchannel cooling device optimization.

- The buoyancy force effect can be investigated in smaller hydraulic diameters in order to detect a threshold hydraulic diameter defining the conditions where the buoyancy force can be ignored.

- The flow characteristics at the exit of the inlet orifice in vertical upward and downward flow direction need to be visually investigated if any specific phenomena lead to flow oscillation control differences.

- Almost all flow instability investigations in microchannel(s) are in straight geometry. The curved configuration can be a novel direction to be investigated for future design. Since the flow behaviors and the heat transfer are quite different in curved configurations due to the secondary flow effect, the flow instability characteristics may be different to the case with a straight tube. The inlet orifice effect also can be studied for curved tubes.

Publications

Journal Papers

1. You, Q, Hassan, I. and Kadem, L., 2014, "Experimental Investigation of Flow Boiling Instability in a Single Microtube with and without an Inlet Orifice", Journal of Heat Transfer, submitted.

2. You, Q., Hassan, I. and Kadem, L, 2014, "Experimental Investigation on Flow Instability in a Single Vertical Microtube with Different Hydraulic Diameters", Journal of Heat Transfer, submitted.

Conferences

1. You, Q., Hassan, I. and Kadem L., "Experimental Investigation on Flow Instability in a Single Vertical Microtube", ASME 2015 13th International Conference on Nanochannels, Microchannels and Minichannels, San Francisco, CA, USA, July 6 - 9, 2015, submitted.

2. You, Q., Hassan, I. and Kadem L., "Effect of Hydraulic Diameter on Flow Boiling Instability in a Single Microtube with Vertical Upward Flow", 2015 the 2nd International Conference on Fluid Flow, Heat and Mass Transfer, Ottawa, Canada, April 30 – May 1, 2015, submitted.

3. You, Q., Hassan I. and Fan, Y.F., "Experimental Measurement of Single-phase Liquid Heat Transfer in a Curved Microtube Using Thermochromic Liquid Crystal", 2015 the 2nd International Conference on Fluid Flow, Heat and Mass Transfer, Ottawa, Canada, April 30 – May 1, 2015, submitted.

Reference

Ali, R., Palm, B., Martin-Callizo, C. and Maqbool, M. H., 2013, "Study of flow boiling characteristics of a microcahnnel using high speed visualization", Journal of Heat Transfer, 135, pp. 081501 (8 pp.).

Barber, J. Brutin, D., Sefiane, K. and Tadrist, L., 2010, "Bubble confinement in flow boiling of FC-72 in a "rectangular" microchannel of high aspect ratio", Experimental Thermal of Fluid Science, 34, pp. 1375-1388.

Bogojevic, D., Sefiane, K., Duursma, G. and Walton, A.J., 2013, "Bubble dynamics and flow boiling instabilities in microchannels", International Journal of Heat and Mass Transfer, 58, pp. 663-675.

Boure, J. A., Bergles, A. E. and Tong, L. S., 1973, "Review of two-phase flow instability", Nuclear Engineering and Design, 25, pp. 165-192.

Brutin, D., Topin, F. and Tadrist, L., 2003, "Experimental study of unsteady convective boiling in heated minichannels", International Journal of Heat and Mass Transfer, 46, pp. 2957-2965.

Brutin, D. and Tadrist, L., 2004, "Pressure drop and heat transfer analysis of flow boiling in a minichannel: influence of the inlet condition on two-phase flow stability", International Journal of Heat and Mass Transfer, 47, pp. 2365-2377.

Celata, G. P., Saha, S. K., Zummo, G. and Dossevi, D., 2010, "Heat transfer characteristics of flow boiling in a single horizontal microchannel", International Journal of Thermal Science, 49, pp. 1086-1094.

Chen, L., Tian, Y. S. and Karayiannis, T. G., 2006, "The effect of tube diameter on vertical two-phase flow regimes in small tubes", International Journal of Heat and Mass Transfer, 49, pp. 4220-4230.

Edel, Z. J. and Mukherjee, A., 2011, "Experimental investigation of vapor bubble growth during flow boiling in a microchannel", International Journal of Multiphase Flow, 37, pp. 1257-1265.

Fan, Y. F. and Hassan, I., 2012, "Experimental investigation of flow boiling instability in a single horizontal microtube with and without inlet restriction", Journal of Heat Transfer, 134, pp. 081501 (11 pp.).

Fan, Y. F., 2013, "Experimental Investigations of Flow Boiling Heat Transfer and Flow Instability in a Horizontal Microtube with an Inlet Orifice", PhD Thesis, Concordia University.

Fan, Y. F and Hassan, I., 2014, "Prediction of the onset of flow instability in a single horizontal microtube with an inlet orifice", Journal of Heat Transfer, 136, pp. 022903 (10 pp.).

Harirchian, T. and Garmella, S. V., 2009, "Effects of channel dimension, heat flux, and mass flux on flow boiling regimes in microchannels", International Journal of Multiphase Flow, 35, pp. 349-362.

Hetsroni, G., Mosyak, A., Pogrebnyak, E. and Segal, Z., 2006, "Periodic boiling in parallel micro-channels at low vapor quality", International Journal of Multiphase Flow, 32, pp. 1141-1159.

Huh, C., Kim, J. and Kim, M. H., 2007, "Flow pattern transition instability during flow boiling in a single microchannel", International Journal of Heat and Mass Transfer, 50, pp. 1049-1060.

Kadam, S. T., Baghel, K. and Kumar, R., 2014, "Simplified Model for Prediction of Bubble Growth at Nucleation Site in Microchannels", Journal of Heat Transfer, 136, pp. 061502 (8 pp.)

Kadlikar, S.G., 2014, "Heat transfer and fluid flow in minichannels and microchannels (second edition)", Butterworth-Heinemann, Oxford, Chapter 3 and Chapter 5

Kandlikar, S. G. and Balasubramanian, P., 2005, "An experimental study on the effect of gravitational orientation on flow boiling of water in 1054X197μm parallel minichannels", Journal of Heat Transfer, 127, pp. 820-829.

Kandlikar, S. G., Willistein, D. A. and Borrelli, J., 2005, "Experimental evaluation of pressure drop elements and fabricated nucleation sites for stabilizing flow boiling in minichannels and microchannels", Proceedings of 3rd International Conference on Microchannels and Minichannels, pp. 115-124.

Kandlikar, S.G., 2010, "Scale effects on flow boiling heat transfer in microchannel: a fundamental perspective", International Journal of Thermal Science, 49, pp. 1073-1085.

Kennedy, J. E., Roach, Jr. G. M., Adbel-Khalik, S. I., Ghiaasiaan, S. M., Jeter, S. M. and Quershi, Z. H., 2000, "The onset of flow instability in uniformly heated horizontal microchannels", Journal of Heat Transfer, 122, pp.118-125.

Lee, S. C. and Bankoff, S. G., 1993, "Prediction of the onset of flow instability in transient subcooled flow boiling", Nuclear Engineering and Design, 139, pp.149-159.

Levy, S., 1967, "Forced convection subcooled boiling – prediction of vapor volumetric fraction", International Journal of Heat and Mass Transfer, 10, pp. 951-965.

Martin-callizo, C., Palm, B., Owhaib, W. and Ali, R., 2010, "Flow boiling visualization of R-134a in a vertical channel of small diameter", Journal of Heat Transfer, 132, pp. 031503 (8 pp.).

Miyata, K., Mori, H., Ohishi, K. and Hamamoto, Y., 2008, "Boiling heat transfer and pressure drop of a refrigerant flowing in a vertical small diameter tube", Proceedings of Internal Refrigeration and Air Conditioning Conference at Purdue, pp. 2421 (8 pp.)

Moffat, R. J., 1988, "Describing the uncertainties in experimental results", Experimental Thermal and Fluid Science, 1, pp. 3-17.

Mudawar, I., 2011, "Two-phase microchannel heat sinks: theory, applications, and limitations", Journal of Electronic Packaging, 133, pp. 041002 (31 pp.).

Mukherjee, A. and Kandlikar, S. G., 2009, "The effect of inlet constriction on bubble growth during flow boiling in microchanels", International Journal of Heat and Mass Transfer, 52, pp. 5204-5212.

Park, J. E., Thome, J. R., and Michel, B., 2009, "Effect of inlet orifice on saturated CHF and flow visualization in multi-microchannel heat sinks", 2009 25th Annual IEEE Semiconductor Thermal Measurement and Management Symposium, pp. 1-8.

Qi, S. L., Zhang, P., Wang, R. Z. and Xu, L. X., 2007, "Flow boiling of liquid nitrogen in micro-tubes: Part I – The onset of nucleate boiling, two-phase flow instability and two-phase flow pressure drop", International Journal of Heat and Mass Transfer, 50, pp. 4999-5016.

Qu, W. and Mudawar, I., 2003, "Measurement and prediction of pressure drop in two-phase micro-channel heat sinks", International Journal of Heat and Mass Transfer, 46, pp.2737-53.

Roach, Jr. G. M., Adbel-Khalik, S. I., Ghiaasiaan, S. M., Dowling, M. F. and Jeter, S. M., 1999, "Low-flow onset of flow instability in heated microchannels", Nuclear Science and Engineering, 133, pp. 106-117.

Schneider, B., Kosar, A. and Peles, Y., 2007, "Hydrodynamic cavitation and boiling in refrigerant (R-123) flow inside microchannels", International Journal of Heat and Mass Transfer, 50, pp. 2838-2854.

Shuai, J. Y., Kulenovic, R., Mertz, R. and Groll, M., 2002, "Experiemental investigation of flow boiling in vertical microchannels", Archives of Thermodynamics, 23, pp. 39-48.

Sobierska, E., Kulenovic, R., Mertz, R. and Groll, M., 2006, "Experimental results of flow boiling of water in a vertical microchannel", Experimental Thermal and Fluid Science, 31, pp. 111-119

Sobierska, E., Kulenovic, R. and Mertz, R., 2007, "Heat transfer mechanism and flow pattern during flow boiling of water in a vertical narrow channel-experimental results", International Journal of Thermal Science, 46, pp. 1172-1181

Steinke, M. E. and Kandlikar, S. G., 2004, "An experimental investigation of flow boiling characteristics of water in parallel microchannels", Journal of Heat Transfer, 126, pp. 518- 526.

Tibirica, C. B. and Ribatski, G, 2014, "Flow patterns and bubble departure fundamental characteristics during flow boiling in microscale channels", Experimental Thermal and Fluid Science, http://dx.doi.org/10.1016/j.expthermflusci.2014.02.017

Stenning, A. H ., 1964, "Instabilities in flow of boiling liquid", Transactions – Journal of Basic Engineering, 86, pp. 213-217

Wang, C. C., Chang, W. J., Dai, C. H., Lin, Y. T. and Yang, K. S., 2012, "Effect of inclination on the convective boiling performance of a microchannel heat sink using HFE-7100", Experimental Thermal and Fluid Science, 36, pp. 143-148.

Wang, G. and Cheng, P., 2008, "An experimental study of flow boiling instability in a single microchannel", International Communications in Heat and Mass Transfer, 35, pp. 1229-1234.

Wang, G., Cheng, P. and Wu, H., 2007, "Unstable and stable flow boiling in parallel microchannels and in a single microchannel", International Journal of Heat and Mass Transfer, 50, pp. 4297-4310

Wang, G., Cheng, P. and Bergles, A. E., 2008, "Effects of inlet/outlet configurations on flow boiling instability in parallel microchannels", International Journal of Heat and Mass Transfer, 51, pp. 2267-2281.

Wang, J., Huang, Y. and Wang, Y., 2011b, "Visualized study on specific points on demand curves and flow patterns in a single-side heated narrow rectangular channel", International Journal of Heat and Mass Transfer, 32, pp.982-992.

Wang, Q., Chen, J. X, Kakac, S. and Ding, Y., 1994, "An experimental investigation of density-wave-type oscillations in a convective boiling upflow system", International Journal of Heat and Fluid Flow, 15, pp. 241-246.

Wang, Y., Sefiane, K and Bennacer, R., 2011a, "Investigation of boiling and bubble confinement in a high aspect ratio micro-channel", Applied Thermal Engineering, 31, pp. 610-618.

Wu, H. Y. and Cheng, P., 2003, "Visualization and measurements of periodic boiling in silicon microchannels", International Journal of Heat and Mass Transfer, 46, pp. 2603-2614.

Whittle, R. H. and Forgan, R., 1967, "A correlation for the minima in the pressure drop versus flow-rate curves for sub-cooled water flowing in narrow heated channels", Nuclear Engineering and Design, 6, pp. 89-99.

Xu, J., Zhou, J. and Gan, Y., 2005, "Static and dynamic flow instability of a parallel microchannel heat sink at high heat fluxes", Energy conversion and management, 46, pp. 313-334.

Yin, L., Jia, L., Guan, P. and Liu, D., 2014, "Experimental investigation on bubble confinement and elongation in microchannel flow boiling", Experimental Thermal and Fluid Science, 54, pp. 290-296.

Zhang, H.Y., Pinjala, D. and Wong, T. N., 2005, "Experimental characterization of flow boiling heat dissipation in a microchannel heat sink with different orientations", Proceedings of 7th Electronic Packaging Technology Conference, pp.670-676.

Appendix A: Saturated properties of

FC-72

P (kPa)	T_{sat} (°C)	C_p (J/kgK)	h_{fg} (J/kg)	μ (Pa·s)	ρ_f (kg/m3)	ρ_v (kg/m3)
8.61	0	1011	99182	9.50E-04	1755	1.37
11.6	5	1019	98000	8.74E-04	1738	1.8
14.6	10	1026	96818	8.00E-04	1720	2.23
19	15	1034	95593	7.43E-04	1706	2.86
23.5	20	1042	94369	6.87E-04	1692	3.48
30	25	1050	93094	6.44E-04	1680	4.36
36.6	30	1057	91820	6.01E-04	1669	5.23
45.7	35	1065	90497	5.68E-04	1659	6.41
54.7	40	1073	89174	5.35E-04	1650	7.59
67.2	45	1080	87789	5.09E-04	1641	9.14
79.5	50	1088	86404	4.83E-04	1631	10.7
96	55	1096	84970	4.61E-04	1623	12.7
101	56.6	1098	84511	4.54E-04	1620	13.4
112	60	1104	83536	4.39E-04	1614	14.8
134	65	1111	82046	4.18E-04	1603	17.5
155	70	1119	80557	3.98E-04	1593	20.2
182	75	1127	79024	3.80E-04	1581	23.7
209	80	1135	77492	3.62E-04	1569	27.2
243	85	1142	75928	3.43E-04	1554	31.6
276	90	1150	74365	3.25E-04	1539	36
317	95	1158	72783	3.20E-04	1520	41.5
359	100	1165	71201	3.14E-04	1501	47
409	105	1173	69447	3.08E-04	1477	53.8
459	110	1181	67693	3.03E-04	1453	60.6
519	115	1189	65994	2.96E-04	1424	69.1
579	120	1196	64295	2.90E-04	1394	77.5
650	125	1204	62215	2.82E-04	1357	88
721	130	1212	60134	2.74E-04	1321	98.6
805	135	1219	57642	2.65E-04	1277	112
889	140	1227	55149	2.56E-04	1233	126
987	145	1235	52059	2.45E-04	1180	144
1085	150	1243	48969	2.34E-04	1128	162

Appendix B: Drawings

B 1: Support Drawing
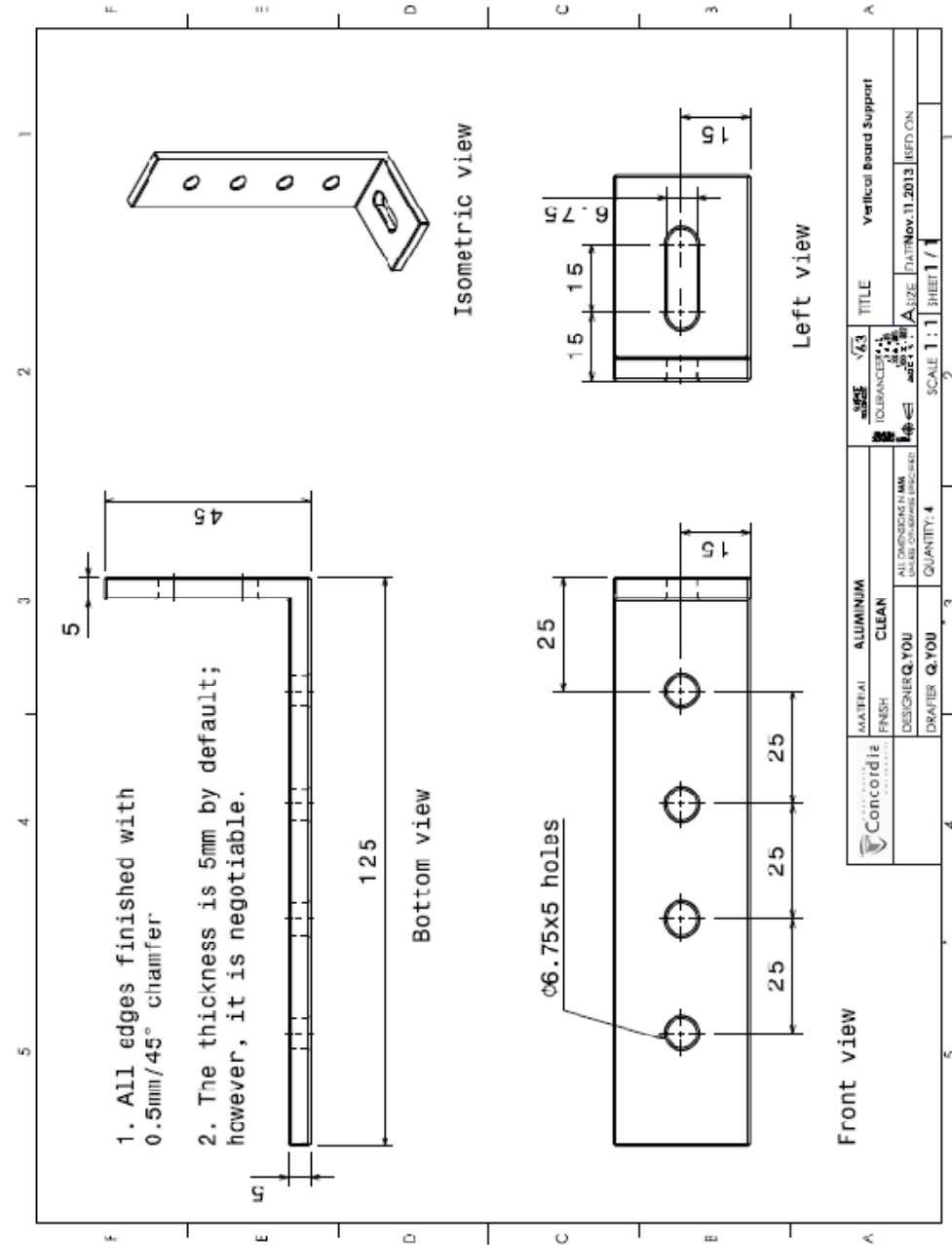
B 2: Vertical Board Drawing

1. All edges finished with 0.5mm/45° chamfer

2. The thickness is 5mm by default; however, it is negotiable.

Φ6.75x110 holes on 25mm grid

R18

20

87.5

175

500

Front view

Left view

5

MATERIAL ALUMINIUM
FINISH CLEAN
DESIGNER Q.YOU
DRAFTER Q.YOU

Concordia

ALL DIMENSIONS IN MM
UNLESS OTHERWISE SPECIFIED
QUANTITY: 1

TITLE Vertical Board

A SIZE DATE Nov.1.2013 USED ON
SHEET 1/1
SCALE 1 : 1

88

Appendix C: Dominant frequency

(MATLAB program– FFT analysis)

```
close all;
clear all;
clc;


samples = xlsread('Pin.xlsx'); %Experment results

fs = 400; %sampling frequency (Hz)

fnyquist = fs/2;

N = length (samples);


fax_bins = [1:N];
fax_Hz = fax_bins*fs/N;

y = (abs(fft(samples)))';
setup = [fax_Hz; y]';
setup = setup(1:N/4,:);

plot(fax_Hz, y); %power spectral density figure (the frequency
spectrum)

xlabel ('Frequency (Hz)', 'FontName','Times New Roman', 'FontSize',
32);
ylabel ('Magnitude', 'FontName','Times New Roman', 'FontSize', 32);
axis([0 5 0 5*10^4]);
set(gca,'FontName','Times New Roman', 'Fontsize',28)
title ('Pin - Frequency Spectrum', 'FontName','Times New Roman',
'FontSize', 50);
```

Appendix D: Heat loss evaluation

A heat loss function is built as a relationship between tube wall temperatures and applied energy on the empty microtube. During flow boiling experiments, an average wall temperature for each test matrix is recorded and substituted into the heat loss function created before. Therefore, the heat flux applied on the channel surface can be obtained by subtracting the heat loss from the total power applied,

$$q'' = \frac{VI}{\pi D_h L_h} - q''_{loss}$$

Tube size	Maximum heat loss % of total heat flux applied
Tube L	4%
Tube M	11%
Tube S	15%

Appendix E: Samples of calculated uncertainties

1. Uncertainty of inlet orifice area ratio ($\delta AR\%$)

    Given: 50% inlet orifice;

    $D_o = 0.635$ mm, $\delta D_o = \pm 0.0127$ mm;

    $D_h = 0.889$ mm, $\delta D_h = \pm 0.0127$ mm.

    Calculated:

    $$AR\% = \frac{D_o^2}{D_h^2} \times 100\% \tag{0.1}$$

    $$\delta AR\% = \sqrt{\left(\delta D_o \frac{\partial AR\%}{\partial D_o} \right)^2 + \left(\delta D_h \frac{\partial AR\%}{\partial D_h} \right)^2} \tag{3.4}$$

    $$\delta AR\% = \sqrt{\left(\delta D_o \frac{2 D_o}{D_h^2} \times 100\% \right)^2 + \left(\delta D_h \frac{-2 D_o^2}{D_h^3} \right)^2}$$

    $$= \sqrt{\left(0.0127 \times \frac{2 \times 0.635}{0.889^2} \times 100\% \right)^2 + \left(0.0127 \times \frac{2 \times 0.635^2}{0.889^3} \times 100\% \right)^2}$$

    $$= \pm 2.5\%$$

2. Uncertainty of pressure drop ($\delta \Delta P$)

    Given: P_{in} (full scale) = 517 kPa (75 psi), $\delta P_{in} = \pm 0.259$ kPa;

    P_{out} (full scale) = 345 kPa (50 psi), $\delta P_{out} = \pm 0.173$ kPa.

    Calculated:

    $$\Delta P = P_{in} - P_{out}$$

    $$\delta \Delta P = \sqrt{\left(\delta P_{in} \right)^2 + \left(\delta P_{out} \right)^2} \tag{3.5}$$

    $$\delta \Delta P = \sqrt{\left(0.259 \right)^2 + \left(0.173 \right)^2} = \pm 0.311 \text{kPa}$$

3. Uncertainty of mass flux (δG)

Given: Rotameter 2 ($G = 1400$ kg/m^2·s)

$T_{in} = 24$ °C, $\delta T_{in} = \pm 0.5$ °C;

$Q = 5.45 \times 10^{-7}$ m^3/s, $\delta Q = \pm 2.73 \times 10^{-8}$ m^3/s;

$D_h = 8.89 \times 10^{-4}$ m, $\delta D_h = \pm 1.27 \times 10^{-5}$ m.

Calculated:

$$G = \rho \frac{Q}{A}$$

$$\rho = 1760 - 2.61T \qquad \text{(3M Company)}$$

$$A = \frac{\pi D_h^{\,2}}{4}$$

$$G = (1760 - 2.61T)\frac{Q}{\dfrac{\pi D_h^{\,2}}{4}}$$

$$\frac{\partial G}{\partial T} = (-2.61)\frac{Q}{\dfrac{\pi D_h^{\,2}}{4}} = (-2.61)\times \frac{5.45 \times 10^{-7}}{\dfrac{\pi}{4}\times (8.89 \times 10^{-4})^2} = -2.293$$

$$\frac{\partial G}{\partial Q} = \frac{(1760 - 2.61T)}{\dfrac{\pi D_h^{\,2}}{4}} = \frac{(1760 - 2.61 \times 24)}{\dfrac{\pi}{4}\times (8.89 \times 10^{-4})^2} = 2.73 \times 10^9$$

$$\frac{\partial G}{\partial D_h} = (-2)\times \frac{(1760 - 2.61T)Q}{\dfrac{\pi D_h^{\,3}}{4}} = (-2)\times \frac{(1760 - 2.61 \times 24)\times 5.45 \times 10^{-7}}{\dfrac{\pi}{4}\times (8.89 \times 10^{-4})^3} = -3.355 \times 10^6$$

$$\delta G = \sqrt{\left(\delta T \frac{\partial G}{\partial T}\right)^2 + \left(\delta Q \frac{\partial G}{\partial Q}\right)^2 + \left(\delta D_h \frac{\partial G}{\partial D_h}\right)^2} \qquad (3.6)$$

$$\delta G = \sqrt{(0.5 \times -2.239)^2 + (2.73 \times 10^{-8} \times 2.73 \times 10^9)^2 + (1.27 \times 10^{-5} \times -3.355 \times 10^6)^2} = 85.9 \, \text{kg/m}^2 \cdot \text{s}$$

$$\frac{\delta G}{G} = \frac{85.9}{1400} = 6\%$$

4. Uncertainty of heat flux ($\delta q''$)

Given: V = 2.375V, $\delta V = \pm 0.05$ V;

    I = 8.3A, $\delta I = \pm 0.05$ A;

    $D_h = 8.89 \times 10^{-3}$ cm, $\delta D_h = \pm 1.27 \times 10^{-3}$ cm;

    $L_h = 10$ cm, $\delta L_h = \pm 0.1$ cm.

Calculated:

$$q'' = \frac{V \cdot I}{A_{surface}} = \frac{V \cdot I}{\pi D_h L_h}$$

$$\frac{\partial q''}{\partial V} = \frac{I}{\pi D_h L_h} = \frac{8.3}{\pi \times 8.89 \times 10^{-3} \times 10} = 2.972$$

$$\frac{\partial q''}{\partial I} = \frac{V}{\pi D_h L_h} = \frac{2.375}{\pi \times 8.89 \times 10^{-3} \times 10} = 0.850$$

$$\frac{\partial q''}{\partial D_h} = -\frac{V \cdot I}{\pi D_h^2 L_h} = \frac{2.375 \times 8.3}{\pi \times (8.89 \times 10^{-3})^2 \times 10} = -79.394$$

$$\frac{\partial q''}{\partial L_h} = -\frac{V \cdot I}{\pi D_h L_h^2} = \frac{2.375 \times 8.3}{\pi \times 8.89 \times 10^{-3} \times (10)^2} = -0.7058$$

$$\delta q'' = \sqrt{\left(\delta V \frac{\partial q''}{\partial V}\right)^2 + \left(\delta I \frac{\partial q''}{\partial I}\right)^2 + \left(\delta D_h \frac{\partial q''}{\partial D_h}\right)^2 + \left(\delta L_h \frac{\partial q''}{\partial L_h}\right)^2} \qquad (3.7)$$

$$\delta q'' = \sqrt{(0.05 \times 2.972)^2 + (0.05 \times 0.850)^2 + (1.27 \times 10^{-3} \times -79.394)^2 + (0.1 \times -0.7058)^2}$$
$$= \pm 0.20 \, \text{W/cm}^2$$

Appendix F: Experimental data

F.1: Tube L (without inlet orifice)

	G(kg/m²·s)	V(V)	I(A)	q"(W/cm²)	f(Hz)	AMP(kPa)	MAG(kPa)	
	701	2.375	8.30	6.9	0.022	8.03	17.12	OFI
	867	2.420	8.51	7.2	0.670	5.94	19.66	OFI
VU	997	2.510	8.82	7.7	0.060	12.70	16.58	OFI
	1192	2.620	9.10	8.4	0.037	8.88	15.98	OFI
	1396	2.780	9.61	9.4	0.040	5.66	17.63	OFI
	701	1.980	6.95	4.7	0.240	5.27	21.04	OFI
VD	867	2.245	7.90	6.2	0.440	8.35	24.54	OFI
	997	2.410	8.45	7.1	0.020	15.00	22.03	OFI
	1192	2.655	9.28	8.6	0.020	16.97	24.08	OFI

F.2: Tube M (without inlet orifice)

	G(kg/m^2·s)	V(V)	I(A)	q"(W/cm^2)	f(Hz)	AMP(kPa)	MAG(kPa)	
	708	1.480	3.20	2.6	2.7	1.98	16.23	OFI
	852	1.670	3.55	3.2	4.1	2.14	18.79	OFI
VU	996	1.790	3.85	3.8	4.6	2.28	21.13	OFI
	1194	1.990	4.25	4.7	5.1	1.93	24.30	OFI
	1401	2.200	4.75	5.9	5.0	2.03	33.65	OFI
	708	1.355	2.95	2.1	0.01	0.40	17.88	Transient
	852	1.510	3.33	2.7	0.01	0.51	24.38	Transient
VD	996	1.679	3.60	3.3	0.01	0.32	29.12	Transient
	1194	1.868	4.00	4.1	0.01	0.27	32.39	Transient
	1401	2.070	4.45	5.2	0.01	0.39	41.20	Transient

F.3: Tube S (without inlet orifice)

	G(kg/m^2·s)	V(V)	I(A)	q"(W/cm^2)	f(Hz)	AMP(kPa)	MAG(kPa)	
	846	1.076	2.06	2.0	0.01	1.98	16.23	Transient
	1011	1.133	2.19	2.2	0.01	2.14	18.79	Transient
VU	1204	1.203	2.30	2.5	0.01	2.28	21.13	Transient
	1397	1.249	2.40	2.7	0.01	1.93	24.30	Transient
	1617	1.320	2.55	3.1	0.01	2.03	33.65	Transient
	846	1.024	2.00	1.8	-	-	-	Blockage
	1011	1.086	2.11	2.0	-	-	-	Blockage
VD	1204	1.175	2.25	2.4	-	-	-	Blockage
	1397	1.238	2.40	2.7	-	-	-	Blockage
	1617	1.670	2.45	3.8	-	-	-	Blockage

F.4: Tube L (heat flux effect)

	G(kg/m^2·s)	V(V)	I(A)	q"(W/cm^2)	f(Hz)	AMP(kPa)	MAG(kPa)	
		2.375	8.30	6.9	0.022	8.03	17.12	OFI
	701	2.650	8.99	8.3	0.210	5.23	19.40	FI
		2.770	9.29	9.0	0.810	4.71	19.69	FI
VU		2.510	8.82	7.7	0.060	12.70	16.58	OFI
	997	2.660	9.19	8.6	0.380	12.58	16.05	FI
		2.850	9.59	9.6	0.720	7.02	20.88	FI
		1.980	6.95	4.7	0.240	5.27	21.04	OFI
	701	2.115	7.39	5.4	4.200	2.27	25.47	FI
		2.370	8.20	6.7	-	1.52	25.63	FI
VD		2.410	8.45	7.1	0.016	15.00	22.03	OFI
	997	2.470	8.60	7.4	0.062	13.97	21.64	FI
		2.600	8.80	8.0	0.171	14.28	22.74	FI

F.5: Tube L (with an inlet orifice)

	$G(\text{kg/m}^2\cdot\text{s})$	V(V)	I(A)	$q''(\text{W/cm}^2)$	f(Hz)	AMP(kPa)	MAG(kPa)	
VU	701	2.375	8.30	6.9	0.022	8.03	17.12	w/o (OFI)[1]
		2.450	8.30	6.9	-	1.03	22.90	50%[2]
		2.480	8.30	6.9	-	0.30	28.41	20%[3]
		2.375	8.30	6.9	-	-	22.90	50% (OFI)[4]
	997	2.510	8.82	7.7	0.058	12.70	16.58	w/o (OFI)
		2.594	8.82	7.7	-	-	27.23	50%
		2.646	8.78	7.7	-	-	34.77	20%
		2.780	9.26	9.0	0.037	15.02	22.25	50% (OFI)
	1192	2.620	9.10	8.4	0.037	8.88	15.98	w/o (OFI)
		2.702	9.10	8.4	-	-	23.35	50%
		2.682	9.03	8.4	-	-	40.41	20%
		2.850	9.54	9.5	1.508	2.87	37.35	50% (OFI)
VD	701	1.980	6.95	4.8	0.238	5.27	21.04	w/o (OFI)
		1.973	6.94	4.8	-	-	19.12	50%
		2.064	6.94	4.8	-	-	29.64	20%
		2.015	7.11	5.0	0.353	6.71	21.71	50% (OFI)
	867	2.245	7.90	6.2	0.441	8.35	24.54	w/o (OFI)
		2.258	7.90	6.2	-	-	22.89	50%
		2.364	7.90	6.2	-	-	39.72	20%
		2.304	8.11	6.5	0.065	12.35	23.38	50% (OFI)
	997	2.410	8.45	7.1	0.016	15.00	22.03	w/o (OFI)
		2.410	8.44	7.1	-	-	25.86	50%
		2.517	8.45	7.1	-	-	48.08	20%
		2.635	8.55	7.9	0.027	12.43	24.94	50% (OFI)

[1] set the case without inlet orifice at OFI as the reference;
[2] with 50% inlet orifice, the flow behaviors at the operating conditions same as the reference;
[3] with 50% inlet orifice, the flow behaviors at the operating conditions same as the reference;
[4] with 50% inlet orifice, the OFI.